GFZ
Helmholtz Centre
POTSDAM

GeoMod2014

Modelling in Geosciences

Programme & Extended Abstracts

31 August - 5 September 2014

Editors:
Kirsten Elger
Øystein Thordén Haug
Malte Ritter

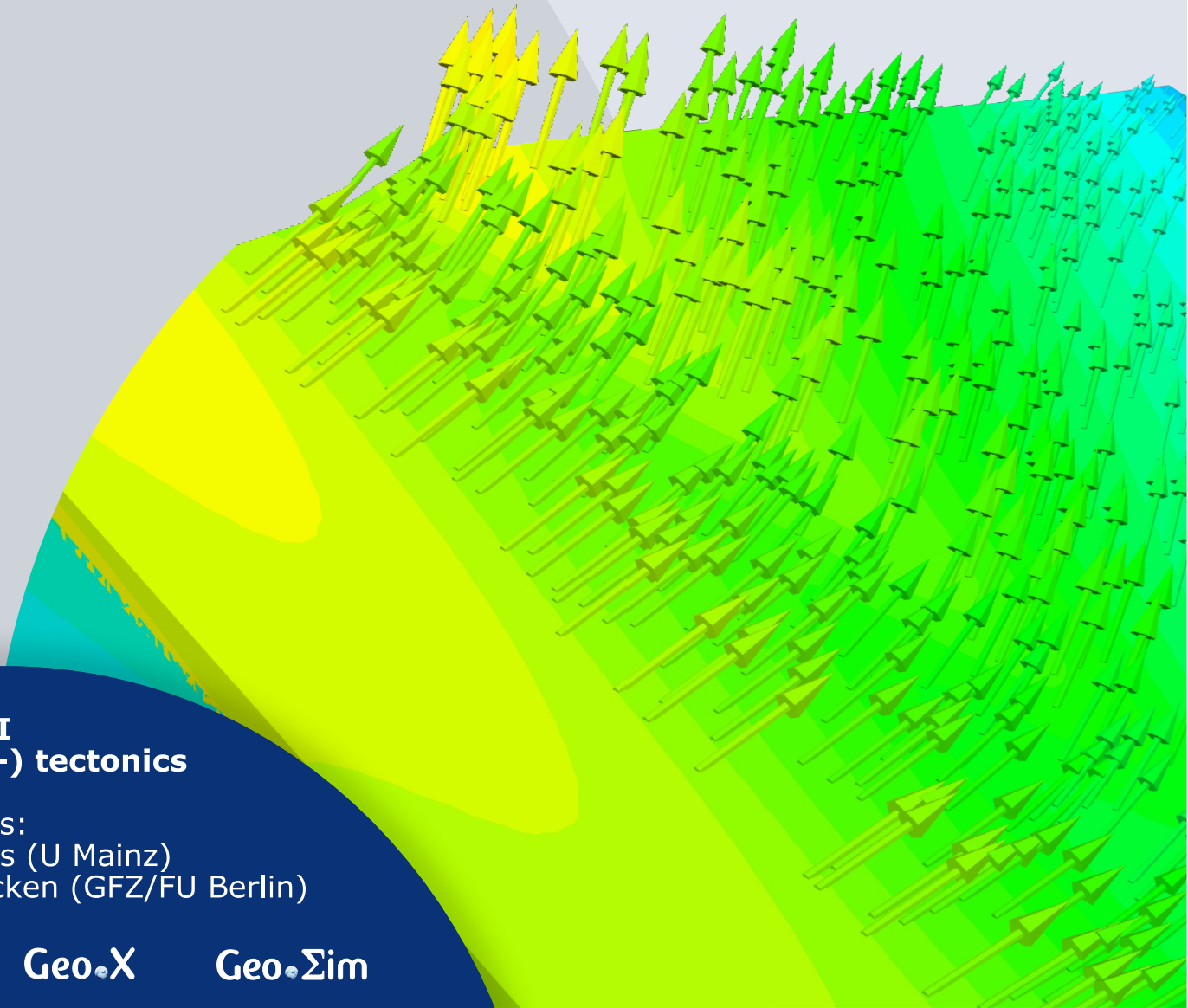

Session I
(Seismo-) tectonics

Conveners:
Boris Kaus (U Mainz)
Onno Oncken (GFZ/FU Berlin)

DFG GeoX GeoSim

Recommended Citation

Elger, K; Haug, Ø. T.; Ritter, M. C. (Eds), (2014): Proceedings of GeoMod2014 – Modelling in Geosciences: Programme and Extended Abstracts 31 August–5 September 2014, GeoMod2014 – Modelling in Geosciences (Potsdam 2014), Potsdam: GFZ German Research Centre for Geosciences. DOI: http://doi.org/10.2312/GFZ.geomod.2014.001.

Disclaimer and Copyright

Imprint

Publisher
Helmholtz Centre Potsdam
GFZ German Research Centre for Geosciences
Telegrafenberg
14473 Potsdam
Published in Potsdam, Germany

Editors
Kirsten Elger
Øystein T. Haug
Malte C. Ritter

doi: 10.2312/GFZ.geomod.2014.001

About this book

This volume contains the extended abstracts of contributions presented during GeoMod 2014 at the Helmholtz Centre Potsdam GFZ German Research Centre for Geosciences (GFZ Potsdam), showing the state of the art of the tectonic modeling community.

GeoMod is a biennial conference dedicated to latest results of analogue and numerical modelling of lithospheric and mantle deformation. It started in 2002 in Milan as RealMod2002, then moved to Lucerne (GeoMod2004), Florence (2008), Lisbon (2010), and Lausanne (2012).

GeoMod2014 took place from 31 August to 3 September 2014 with 138 participants from 25 countries on all continents. The scientific programme of GeoMod2014 was organized in seven topical sessions listed below. The conference was followed by a 2-day short course on "Constitutive Laws: from Observation to Implementation in Models" (including lectures, lab visits, and practical exercises), as well as a 1-day hands-on tutorial on the ASPECT numerical modelling software.

GeoMod2014 focused on rheology and deformation at a wide range of temporal and spatial scales: from earthquakes to long-term deformation, from microstructures to orogens and subduction systems. For the first time, the discipline of volcanotectonics was included, while the (mantle) geodynamics community was more strongly represented than in previous editions. The bridge to field geology has traditionally been strong. At GeoMod 2014, fitting to the focus on rheology, the rock mechanics community was also represented. We thank our sponsors DFG, GFZ Potsdam and Geo.X, the conveners and all participants for contributing to a successful conference.

The GeoMod2014 Committee

The Scientific Committee
Onno Oncken
Georg Dresen
Stephan Sobolev
Matthias Rosenau
Karen Leever

The Organising Committee
Kirsten Elger
Franziska Alberg
Students support: Zahra Amirzada, Felix Eckelmann, Øystein Thordén Haug, Shaoyang Li, Malte Ritter, Tasca Santimano, Sarah Schröder, Johannes Wagner

Sessions, Conveners, and keynote speakers

(Seismo-)tectonics
Conveners: Boris Kaus (U Mainz), Onno Oncken (GFZ/FU Berlin),
Keynotes: Kelin Wang (Geological Survey Canada, Alberta), Bertrand Maillot (U Cergy-Pontoise)

Tectonics & Surface Processes
Conveners: Fabien Graveleau (U Lille), Niels Hovius (GFZ/U Potsdam),
Keynotes: Ritske Huismans (U Bergen), Stéphane Dominguez (U Montpellier II)

Volcanism and Volcanotectonics
Conveners: Olivier Galland (U Oslo), Eoghan Holohan (GFZ)
Keynotes: Rikke Pedersen (U Iceland), Olivier Roche (U BP Clermont-Ferrand)

Geodynamics
Conveners: Francesca Funiciello (U Roma Tre), Stephan Sobolev (GFZ),
Keynotes: Anne Davaille (U Paris-Sud), Bernhard Steinberger (GFZ)

Rheology
Conveners: Georg Dresen (GFZ/U Potsdam), Hiroki Sone (GFZ),
Keynotes: Yuri Fialko (U California), Laurent Montési (U Maryland)

Fluids and Deformation
Conveners: Stephen Miller (U Bonn), Marcos Moreno Switt (GFZ),
Keynotes: Boris Galvan (U Bonn), Takeshi Tsuji (U Kyushu)

Methods and Materials (poster-only session)
Conveners: Matthias Rosenau (GFZ), Marcel Frehner (ETH Zürich)

Short course on "Constitutive Laws: from Observation to Implementation in Models"
Lecturers: Onno Oncken (GFZ Potsdam), Matthias Rosenau (GFZ Potsdam), Fabio Corbi (GFZ Potsdam), Georg Dresen (GFZ Potsdam), Stephan Sobolev (GFZ Potsdam), Sascha Brune (U Sydney)

Hands-on tutorial on "ASPECT: a next-generation geodynamic modelling software"
(Advanced Solver for Problems in Earth's ConvecTion)
Lecturers: Anne Glerum (Utrecht University), Juliane Dannberg (GFZ Potsdam). Supervised by Wolfgang Bangerth (Texas A&M University, ASPECT main developer), Stephan Sobolev (GFZ Potsdam), Bernhard Steinberger (GFZ Potsdam).

Contents

Session I.

(Seismo-)tectonics

Session Description: (Seismo-)tectonics

Conveners: Boris Kaus (U Mainz), Onno Oncken (GFZ/FU Berlin)

In the past decade, several great to giant subduction megathrust earthquakes have occurred (Sumatra 2004 and 2005, Chile 2010 and Japan 2011). Despite the fact that scientists knew that these subduction zones had the potential for megathrust earthquakes each new event had "surprises" in terms of size, duration, and complexity of the rupture, as well as the size of the associated tsunami or upper plate deformation. These events now belong to the group of very densely observed earthquakes, involving pre-seismic, co-seismic and post-seismic observations with integrated instrumentation and field observation encompassing seismology, geodesy, and geomorphology. These investigations have dramatically increased our understanding of the kinematics of the seismic cycle and thrown light on the underlying physical processes. Numerical and physical simulation in particular are benefitting from these results and are beginning to reveal driving mechanisms contributing to an advancement in theoretical understanding. We particularly solicit contributions that add to this development and to an improved understanding of the relationship between deformation accumulation at a wide range of temporal scales.

An investigation of seismicity and lithospheric features of the Zagros region, SW Iran, using coda wave attenuation

Mohsen Ahmadzadeh Irandoust[1], Habib Rahimi[2], Farhad Sobouti[1]

[1] *Department of Earth Sciences, Institute for Advanced Studies in Basic Sciences, Zanjan, Iran*
[2] *Institute of Geophysics, University of Tehran, Tehran, Iran*
e-mail: *m.ahmadzadeh@iasbs.ac.ir*
session: *(Seismo)-tectonics*

Abstract

In this study we used more than 2800 earthquakes to estimate coda wave quality factor, Q_c, in the Zagros Fold and thrust Belt and in the Sanandaj-Sirjan Metamorphic Zone. The coda quality factor was estimated using the single backscattering model. We investigated lateral and depth variation of Q_c in the study region. The average frequency relations for SSZ, Bandar-Abbas region and ZFTB are $Q_c = (124 \pm 5)f^{(0.82\pm0.02)}$, $Q_c = (111 \pm 2)f^{(0.99\pm0.01)}$ and $Q_c = (89 \pm 5)f^{(1.02\pm0.03)}$, respectively. The depth variations of Q_c show that there is a low velocity zone under SSZ and that the lithosphere of NW Zagros is thicker than other parts of ZFTB.
Key words: Quality factor, Attenuation, Seismicity, Coda, Zagros

Introduction

The Zagros mountains of SW Iran are one of the most seismically active intra-continental fold and thrust belts on Earth, and an important element in the active tectonics of the Middle East. Surface faulting associated with earthquakes is extremely rare, and most information about the active faulting comes from earthquakes. Hence, estimation of seismic wave attenuation (Q^{-1}) can be useful for the regions like Zagros. The seismic quality factor (Q) is strongly affected by the tectonic pattern of the lithosphere at any region. The characteristics of seismic coda waves are generally described by the average decay of the envelope in the tail portion of a seismogram. Based on the concept that the earth is assumed to be composed by the randomly distributed heterogeneities, the behavior of coda waves can be adequately explained by the scattering of primary elastic waves in a random medium (Aki and Chouet 1975). The coda quality factor values show frequency dependence as $Q_c = Q_0 f^n$ for $f > 1$ Hz, where Q_0 is Q_c at 1 Hz and n is the frequency relation parameter. Q_0 can be useful to quantify the seismicity of regions. Also n is indicative of the degree of heterogeneity of the crust and varies from 0.5 to 1.1 for most worldwide regions. Higher values of n indicate more heterogeneity and seismicity for a region.

Data and Methodology

In this study we have used over 2800 earthquake records of the Iranian National Seismic Network (INSN) and the Iranian Seismological Center (IRSC) to estimate the coda quality factor (Fig. 1). Features of the data are the following: (1) epicentral distances are less than 100 km, (2) focal depths are less than 20 km, (3) magnitudes are between 2.5 and 5.5, (4) period of data is from 2004 to 2012, and (5) sampling rate of digital seismic data is 50 Hz.

According to the single backscattering model (Aki and Chouet 1975), the coda amplitude can be expressed by $A(f,t) = C(f)t^{-\alpha}exp(-\pi ft/Q_c)$, where $A(f,t)$ is the time series of amplitudes of the

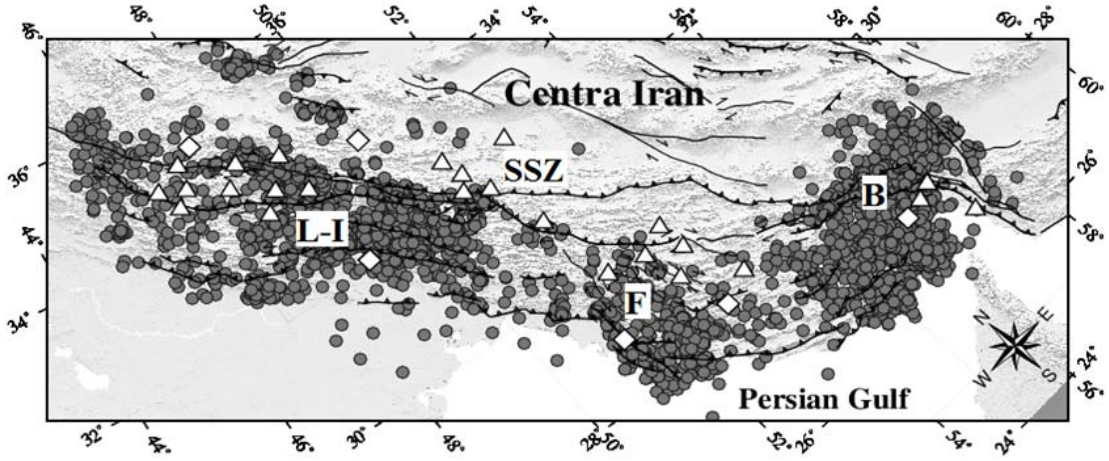

Fig. 1.: Location of stations and earthquakes in Zagros. Subregions of the study region, Bandar-Abbas (B, Fars (F), Lorestan-Izaeh (L-I) and SSZ are shown in the map.

filtered seismograms, $C(f)$ is the coda source factor which is considered as constant and α is the geometrical spreading factor ($\alpha = 1$ for body waves).Taking the natural logarithm of above equation and rearranging the terms, we get, $ln[A(f,t).t] = c - bt$, where $c = lnC(f)$ and $b = \pi f/Q_c$. Filtered seismograms are used for the detailed study of the decay of coda wave amplitudes with time to estimate Q_c values. The signals were filtered in seven frequency windows with central frequencies of 1.5, 3, 4.5, 6, 9, 12 and 18 Hz. To investigate the depth-dependence of attenuation, Q_c values were calculated for 18 lapse times ($5, 10, 15, \ldots$ 90s). Also we used the ellipsoidal volume sampled by coda waves at different lapse times to estimate the maximum scattering depths.

Results and Discussion

To investigate the lateral variation of upper lithosphere attenuation structure, we concentrated on the study of coda waves with shorter lapse times (e.g. 30 s), because they are less affected by deeper parts of the lithosphere. To compare the results in all stations distributed all over the region,Q_0 values are plotted in Fig. 2. In general, it could be seen that the average value of Q_0 in the seismically less active part of the study region, that is, SSZ, is greater than that in the active Zagros region. In the ZFTB there is no significant lateral variation in attenuation, except in the SE Zagros (the Bandar-Abbas region) which shows lower attenuation. The average frequency relations for SSZ, Bandar-Abbas region and ZFTB were obtained as: $Q_c = (124\pm5)f^{(0.82\pm0.02)}$, $Q_c = (111\pm2)f^{(0.99\pm0.01)}$ and $Q_c = (89\pm5)f^{(1.02\pm0.03)}$, respectively.

We have compared some of the results of Q_c studies obtained by various researchers worldwide. Our calculated Q_c values for the study region are comparable with active tectonic regions like Himalaya and SW Anatolia. Among Q_c studies in Iran, SSZ shows the lowest attenuation, while ZFTB shows a high attenuation like Alborz mountains (northern Iran). To investigate the variation of Q_c with depth, we calculated quality factors for 18 lapse time window length. Considering this fact that our study region is very wide and in order to have a good comparison of the spatial attenuation variation between different parts of the Zagros, we divided the region into 4 segments. The subregions are Bandar-Abbas (B), Fars (F), Lorestan-Izeh (L-I) and Sanandaj-Sirjan zone (SSZ) which are shown in Fig. 1. For each subregion, Fig. 3 shows variation of average Q_0 (quality factor at 1 Hz) and n (frequency relation parameter) with respect to lapse time and maximum depth of scattering. The results show that in general, Q_0 is an increasing function of lapse

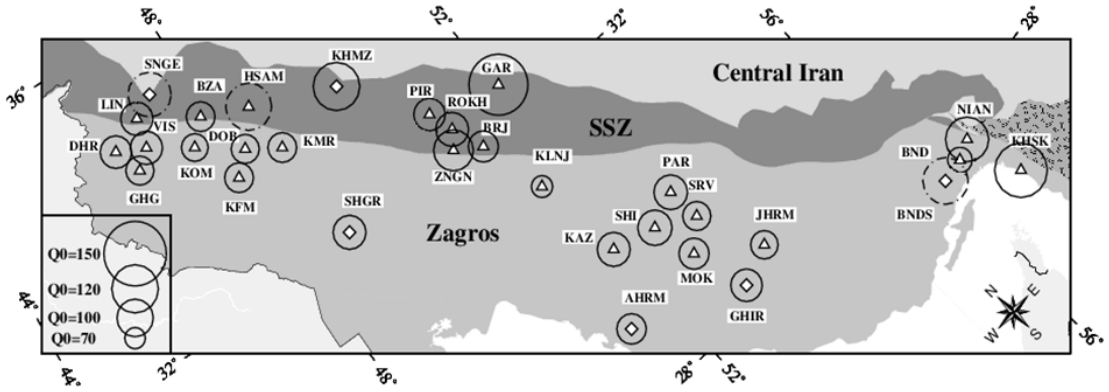

Fig. 2.: Map of Q_0 for 30 s time window lengths. Triangles and diamonds show stations located in Zagros and Sanandaj-Sirjan zone. Inset shows scale for Q_0.

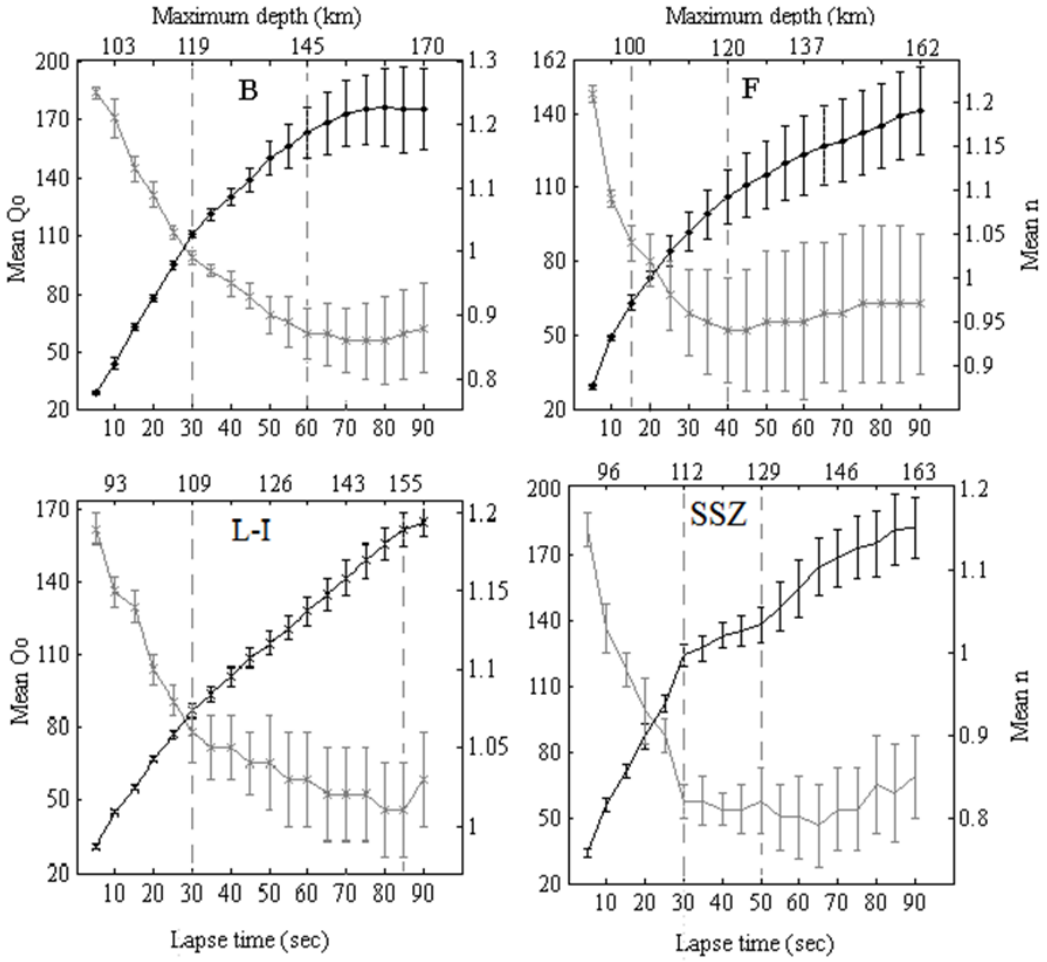

Fig. 3.: Variation of average Q_0, (Q_c in 1 Hz) and n (frequency relation parameter) with lapse time and maximum scattering depth in subregions of the study region, Bandar-Abbas (B), Fars (F), Lorestan-Izaeh (L-I) and Sanandaj-Sirjan Zone (SSZ).

time, while the n value is a decreasing function of lapse time. It seems reasonable that the larger the lapse time indicating the larger the volume of material with larger lateral and depth extent shows higher Q_c and decay of coda at a larger lapse time caries information about attenuation properties of deeper layers of the lithosphere.

Beneath SSZ and at the depth range of 50 to 80 km, there is a high correlation between the previously reported low velocity medium (Kaviani et al. 2007) and the observed sharp changes in the trend of the Q_0 and n curves. In the reported velocity structure in mind, unlike SSZ, under the crust of the Zagros, our results in different parts of the mountain range show no sharp changes in the trends of Q_0 and n. On the other hand, we observe a significant correlation between the reported lithosphere thicknesses (e.g. Priestly et al. 2012) and the trends of Q_0 and n in longer lapse times (i.e. larger depths). The NW Zagros has the thickest lithosphere. In this region the Q_0 curve shows an increasing slope up to a lapse time of 85 s. Other parts of Zagros with thinner lithosphere show a constant or gradually increasing trend of Q_0 and n at large lapse times.

Conclusion

Investigation of the variation of coda wave attenuation in the Zagros region shows our study region is comparable with seismically active tectonic regions of the world. And SSZ shows the lowest attenuation and seismicity among different tectonic areas of Iran. Also there is a correlation between the trends of Q_0 and n we obtained and the reported lithosphere thicknesses and velocity structure in the Zagros region.

References

Aki, K. and Chouet, B., 1975, Origin of coda waves: source, attenuation, and scattering effects, J. geophys. Res., 80, 3322–3342.

Kaviani, A., Paul, A., Bourova, A., Hatzfeld, D., Pedersen, H. and Mokhtari, M., 2007. A strong seismic velocity contrast in the shallow mantle across the Zagros collision zone (Iran), Geophys. J. Int., 171, 399–410.

Priestley, K., McKenzie, D., Barron, J., Tatar, M., and Debayle, E., 2012. The Zagros core: Deformation of the continental lithospheric mantle. Geochemistry, Geophysics, Geosystems, 13(11).

Coseismic Coulomb stress changes on intra-continental normal and thrust faults: insights from three-dimensional finite-element modelling

Meike Bagge[1], Andrea Hampel[1]

[1]*Leibniz Universität Hannover, Institut für Geologie, Callinstraße 30, 30167 Hannover, Germany*
e-mail: *bagge@geowi.uni-hannover.de, hampel@geowi.uni-hannover.de*
session: *(Seismo-) Tectonics*

Investigating the interaction of faults plays a crucial role in the assessment of future seismic risks. The calculation of Coulomb stress changes allows to quantify the stress changes on the so-called receiver faults in the surrounding of the fault that was ruptured during an earthquake. A positive Coulomb stress change implies that the earthquake has brought the receiver fault closer to failure while a negative value indicates a delay of the next earthquake (King et al. 1994; Stein 1999). So far, most studies focussed on calculating the Coulomb stress changes resulting from particular earthquakes such as the 2008 Wenchuan (China) or 2009 L'Aquila (Italy) events (Serpelloni et al. 2012, Parson et al. 2008, Wan & Shen 2010). Furthermore, gravity and the regional stress field were commonly neglected. Here we present a systematic analysis of the Coulomb stress changes on intra-continental dip-slip faults using three-dimensional finite-element models with arrays of normal and thrust faults, respectively. Our models allow the calculation of coseismic ("static") Coulomb stress changes on pre-defined fault planes, whose dip and position relative to each other can be varied. Gravity and a regional stress field are included in the models, which represent a 200 x 200 km wide lithosphere with viscoelastic behaviour of the lower crust and lithospheric mantle (Fig. 1).

Figure 2 shows the vertical and total horizontal coseismic displacement of the model surface and the coseismic total slip on the source fault plane (fault 6). In the thrust fault model, the coseismic

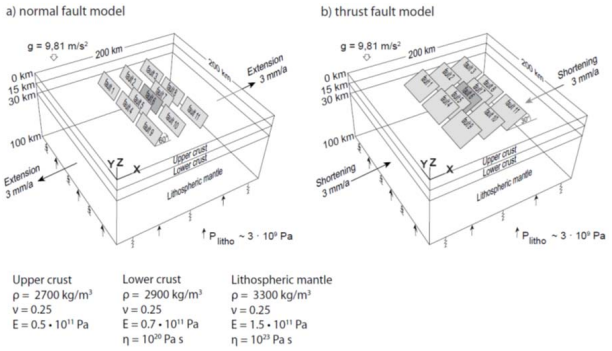

Fig. 1.: Perspective view of the three-dimensional reference model. The lithosphere is divided into an elastic upper crust, viscoelastic lower crust and viscoelastic lithospheric mantle. The source fault (fault 6, dark grey) and the ten receiver faults (light grey) are embedded in the upper crust. The 40-km-long faults dip with 60° in the normal fault reference model (a) and with 30° in the thrust fault reference model (b). The rheological parameters are density (ρ), Young's modulus (E), Poisson's ratio (μ) and viscosity (η). Gravity is included as body force. Isostatic effects are implemented by a lithostatic pressure (P_{litho}, black arrows) and an elastic foundation (springs) representing an asthenosphere. The bottom of the model is free to move in the vertical and horizontal directions and the model sides are fixed in the y-direction. We use a velocity boundary condition to create an extension (a) or shortening (b) of 6 mm/yr in the x-direction to initiate slip on the fault.

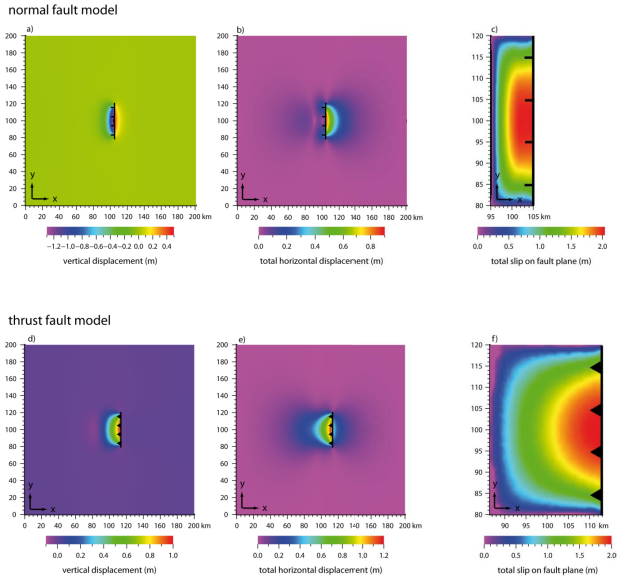

Fig. 2.: Coseismic vertical and total horizontal displacements at the model surface of the normal fault (a, b) and thrust fault (d, e) model. Coseismic slip on the source fault plane (fault 6) in the normal fault (c) and thrust fault (f) model.

vertical displacement shows mainly uplift of the hanging wall (Fig. 2 d). In the normal fault model, subsidence occurs in the hanging wall, whereas uplift is observed in the footwall (Fig. 2 a). The total horizontal displacement is highest in the hanging wall of the thrust fault model (Fig. 2 e) and in the footwall of the normal fault model (Fig. 2 b). Even though the fault planes have a rectangular shape, a typical elliptical slip distribution develops, with 2 m displacement at the surface and zero displacement at the fault tips and downdip edges (Fig. 2 e, f).

In a first series of experiments, we analysed the Coulomb stress changes resulting from coseismic slip of 2 m on the 40-km-long source fault. The preliminary results from both the thrust and normal fault models show that synthetic receiver faults parallel to the source fault experience primarily negative Coulomb stress changes with a symmetric distribution on each fault plane. In other words, these faults are located in a stress shadow zone. In contrast, faults positioned in the along-strike prolongation of the source fault undergo mostly positive Coulomb stress changes, i.e. they are located in a stress triggering zone. The Coulomb stress changes are largest at the fault tip that is closer to the source fault, resulting in an asymmetric Coulomb stress change distribution. Experiments with variable fault dip show that the distribution of the Coulomb stress change depends on the fault dip. Steeper receiver faults generally exhibit smaller Coulomb stress changes than shallow-dipping faults. In the future, we will use the fault-array models to evaluate the Coulomb stress changes arising from postseismic relaxation in the lower crust and lithospheric mantle and their dependence on the viscosity of these layers.

References

King, G. C., Stein, R. S. and Lin, J. (1994): Static stress changes and the triggering of earthquakes. - Bulletin of the Seismological Society of America, 84(3): 935-953.

Parsons, T., Ji, C. and Kirby, E. (2008): Stress changes from the 2008 Wenchuan earthquake and increased hazard in the Sichuan basin. - Nature, 454(7203): 509-510.

Serpelloni, E., Anderlini, L. and Belardinelli, M. E. (2012): Fault geometry, coseismic-slip distribution and Coulomb stress change associated with the 2009 April 6, Mw 6.3, L'Aquila earthquake from inversion of GPS displacements. - Geophysical Journal International, 188(2): 473-489.

Stein, R. S. (1999): The role of stress transfer in earthquake occurrence. - Nature, 402(6762): 605-609.

Wan, Y. and Shen, Z. K. (2010): Static Coulomb stress changes on faults caused by the 2008 Mw 7.9 Wenchuan, China earthquake. - Tectonophysics, 491(1): 105-118.

The role of pre-existing frictional weaknesses on the propagation of extensional fault

Lorenzo Bonini[1], Roberto Basili[2], Pierfrancesco Burrato[2], Vanja Kastelic[2], Giovanni Toscani[1], Silvio Seno[1], Gianluca Valensise[2]

[1] *Dipartimento di Scienze della Terra e dell'Ambiente, Università di Pavia, Italy*
[2] *Istituto Nazionale di Geofisica e Vulcanologia, Rome, Italy*
e-mail: *lorenzo.bonini@unipv.it*
session: *(Seismo-) Tectonics*

Introduction

Understanding the evolution of faults from their blind phase to a mature stage (i. e. surface-breaking faults) is fundamental in active tectonic studies because conventional analyses for identifying and characterizing the earthquake potential of large continental faults rely largely on surface evidence of faults.

In brittle crust, faults form and propagate by linking small tensile cracks. A plethora of studies dealt with fault propagation mechanisms using different approaches, from theoretical formulations to field analyses to numerical and analogue simulations (see Mandl, 2000; Scholz, 2000; and Gudmundsson, 2011 for a summary). In an isotropic material, the propagation of faults is controlled by rock toughness and applied stress. In nature, rocks exhibit intrinsic mechanical anisotropies that affect stress trajectories and consequently the nucleation and growth of faults. Examples of mechanical heterogeneities in nature are lithological changes, layering, fluids, inherited faults etc.

Here we focus on the role that pre-existing thin mechanical discontinuities with different orientations may play in the propagation of an extensional fault. We present a series of clay (wet kaolin) analog models simulating the evolution of a buried extensional structure. To analyze how mechanical discontinuities affect strain distribution and new extensional faults formation, we introduce in the models frictional weaknesses with different orientation (Fig. 1).

Method

Wet clay has been extensively used as analog material since the beginning of experimental geology (see Graveleau et al., 2012 for a review). During the past thirty years, wet kaolin has been selected as the preferred clay type for analogue models because its plasticity index and viscoelasticity are lower than other clay types (Withjack and Jamison, 1986; Eisenstadt and Sims, 2005; Henza et al., 2010; Cooke and van der Elst, 2012). In this study, we use wet kaolin with a density of $1.65\,\mathrm{g\,cm^{-3}}$, a water content of 60 % by mass, a shear strength ranging from 50 Pa to 120 Pa (Eisenstadt and Sims, 2005; Cooke and van der Elst, 2012), and a friction coefficient of 0.6. Under these experimental conditions and following well established scaling rules (e. g. Hubbert, 1937), 1 cm in the experiment is about 1 km in nature. The experimental apparatus simulates extensional displacements of a subsiding rigid block (Fig. 1) at an imposed rate of $0.005\,\mathrm{mm\,s^{-1}}$.

The peculiar properties of wet kaolin allow us to reproduce localized faulting, distributed deformations, and fault reactivation. Recently, Cooke et al., (2013) developed an experimental technique that introduces thin frictional weaknesses in the initial setup of the experiments by

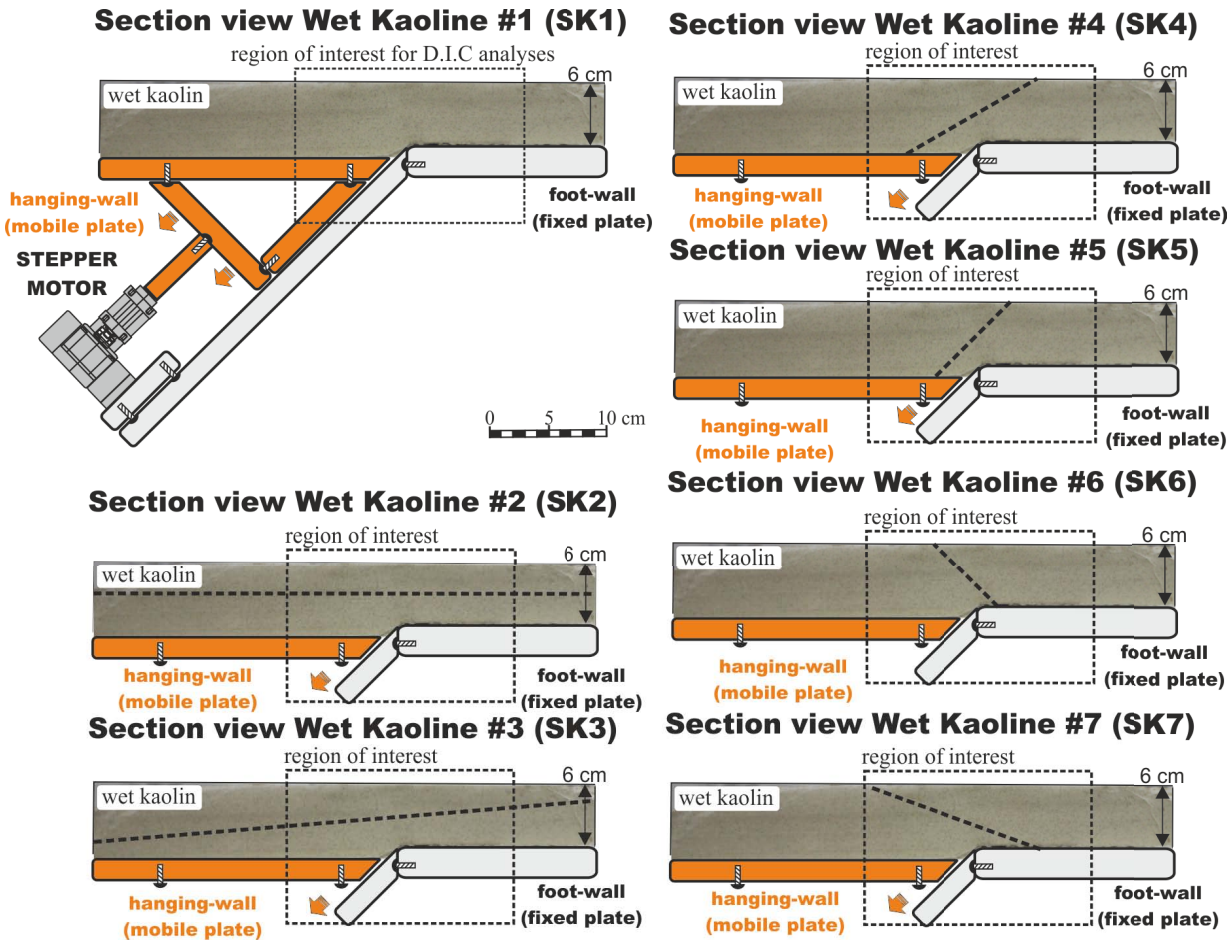

Fig. 1.: Initial setup of the experiments. Dashed lines represent pre-existing mechanical discontinuities introduced in the initial setup.

cutting clay with an electrified blade. The same method has been used by Bonini et al. (2014) in an extensional setting. We use such approach to reproduce pre-existing discontinuities in our models.

To monitor the evolution of the experiments we used an high-resolution camera taking pictures every 0.5 mm of displacement. Then we calculated the strain distribution using the Displacement Image Correlation method (D.I.C.).

Results

In the isotropic experiment (Sk 1), different systems of upward- and downward propagating faults all evolved to form high-angle faults with a listric geometry after 1.5 cm of extension. In all other experiments the results differ depending on the orientation of the mechanical discontinuity. For instance, in the experiments with an horizontal discontinuity (Sk 2) the new fault quickly propagates and buried slip is transferred to the surface by a single fault system after 1 cm of total displacement (0.5 cm before than in Sk 1 model). In the Sk 3 model, the upward-propagating fault slows down its propagation when it meets a low-angle discontinuity. The effect is opposite with respect to Sk 2 model, and a well-developed bending-moment fault appears at the surface of the models. In the Sk 4 model, the discontinuity dips 30°, and when the new upward-propagating fault meets it slip is deflected along it without forming a new fault in the uppermost part of the model. In the Sk 5 model, the initial 45°-dipping discontinuity is quickly reactivated and transfers all the displacement to the surface. Finally, the Sk 6 and Sk 7 experiments simulate inherited antithetic discontinuities; in these models, the upward-propagation of new faults is limited by the inherited discontinuities, and once again bending-moment faults develop at the surface.

Conclusions

Our models show that the nucleation and propagation of extensional faults may be affected differently depending on the orientation of pre-existing frictional weaknesses. The induced tensile stress ahead of upward-propagating faults is influenced by mechanical discontinuities that generate a rotation of the principal stress. This implies differences in (i) the growth rate of the new faults, (ii) the shape of the associated folds, and (iii) the development of bending-moments faults at the surface. In summary, the interaction between new and inherited faults may result (1) in limitations of the size of new structures and, therefore, of the associated earthquakes (down-dip segmentation), and (2) it may cause the reactivation of older fault segments and generate new surface breaks not directly connected to the master faults at depth (bending-moment faults). The 2009 L'Aquila seismic sequence is an example of how seismogenic ruptures on an extensional fault may be strongly controlled at depth by the interaction between new and inherited faults (see Bonini et al., 2014). Other recent damaging earthquakes caused by other types of faults (1983, Coalinga, U.S.A, M_w 6.5; 1989, Loma Prieta, U.S.A., M_w 6.9; 1994, Northridge, U.S.A, M_w 6.7; 2008, Wenchuan, M_w 7.9; 2010, Haiti) also showed a complex multi-level nature of the co- and post-seismic deformations caused by the interaction between seismogenic fault and thin mechanical discontinuities (e. g.: faults, weak layers). The analysis of the relationship between new faults and inherited weaknesses will improve seismic hazard assessment and structural interpretations of seismogenic faults in complex tectonic settings.

Acknowledgements

Work founded by Project Miur-Firb "Abruzzo" (code: RBAP10ZC8K_003)

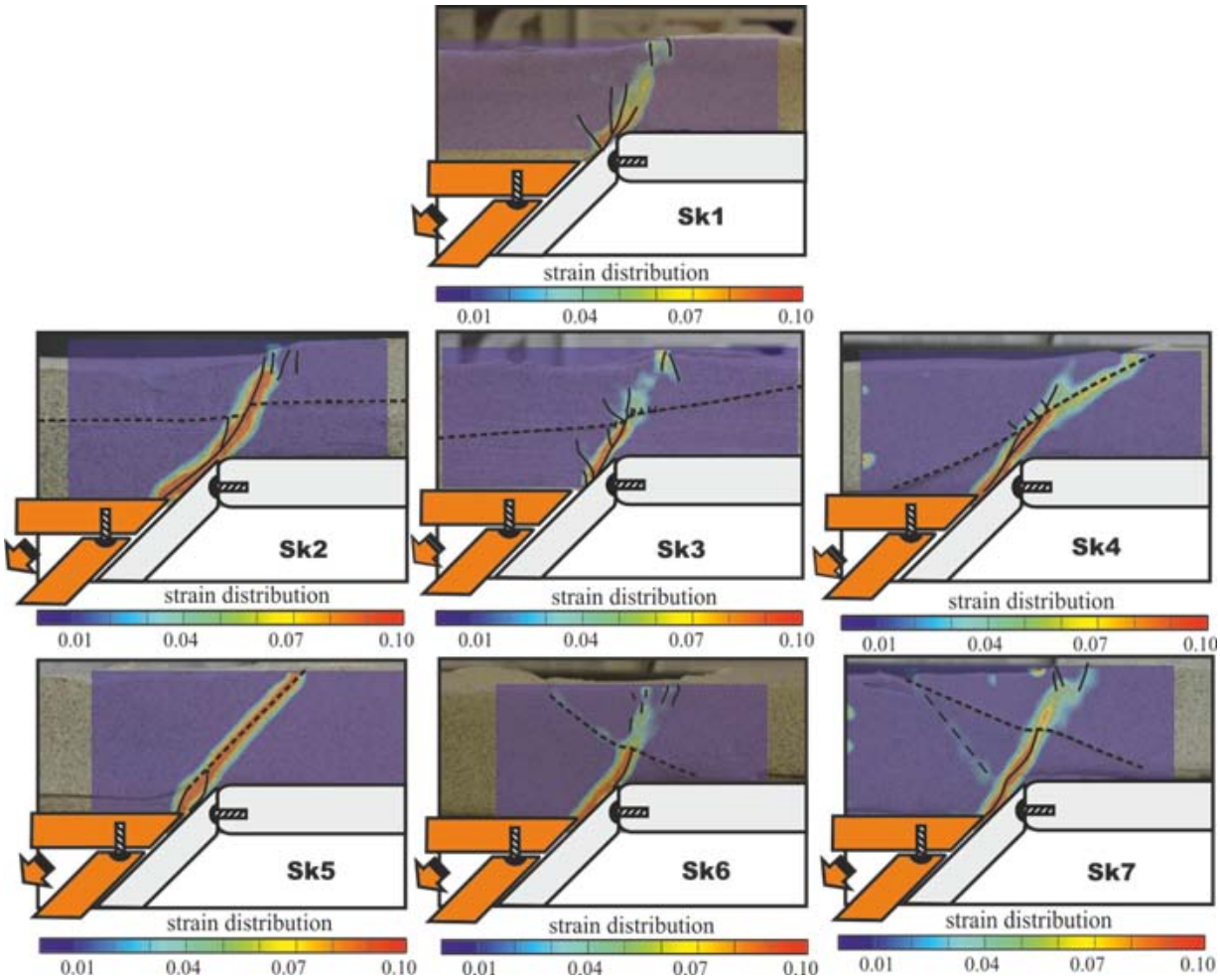

Fig. 2.: The strain distribution in the experiments at 1 cm of total displacement.

References

Bonini, L., Di Bucci, D., Toscani, G., Seno, S., Valensise, G. (2014). On the complexity of surface ruptures during normal faulting earthquakes: excerpts from the 6 April 2009 L'Aquila (central Italy) earthquake (M_w 6.3). Solid earth, 389-408, doi:10.5194/se-5-389-2014.

Cooke, M.L., van der Elst, J. (2012). Rheologic testing of wet kaolin reveals frictional and bi-viscous behavior typical of crustal materials. Geophysical research Letters, 39, L01308, doi:10.1029/2011GL050186.

Cooke, M.L., Schottenfeld, M.T., Buchanan, S.W. (2013). Evolution of fault efficiency at restraining bends within wet kaolin analog experiments. Journal of Structural Geology, 51, 180-192, http://dx.doi.org/10.1016/j.jsg.2013.01.010.

Eisenstadt, G., Sims, D. (2005). Evaluating sand and clay models: do rheological differences matter? Journal of Structural Geology, 27, 1399-1412, doi:10.1016/j.jsg.2005.04.010.

Graveleau, F., Malavieille, J., Dominguez, S. (2012). Experimental modelling of orogenic wedges: A review. Tectonophysics, 538-540, 1-66, doi:10.1016/j.tecto.2012.01.027.

Gudmundsson, A. (2011). Rock fractures in geological processes. Cambrige University Press, New York.

Henza A.A., Withjack, M.O., Schlische, R.W. (2010). Normal-fault development during two phases of non-coaxial extension: An experimental study. Journal of Structural Geology, 32, 1656-1667, doi:10.1016/j.jsg.2009.07.007.

Hubbert, M. K. (1937). Theory of scale models as applied to the study of geologic structures, Geol. Soc. Am. Bull., 48, 1459–1520.

Mandl, G. (2000). Faulting in brittle rocks: an introduction to the mechanics of tectonic faults, Springer Berlin.

Scholz, C. H. (2000). The mechanics of earthquakes and faulting, Cambridge University Press, 439 pp.

Withjack, M.O., Jamison, W.R. (1986), Deformation produced by oblique rifting, Tectonophysics, 126, 99–124, doi:10.1016/0040-1951(86)90222-2.

Analogue models of subduction megathrust earthquakes: analyzing the viscoelastic rheological parameter space with an innovative monitoring technique

Silvia Brizzi[1], Fabio Corbi[1, 2], Francesca Funiciello[1], Monica Moroni[3]

[1] *Dipartimento di Scienze, Sezione di Geologia, Università degli Studi "Roma Tre", L.go S. Leonardo Murialdo, I – 00146, Rome, Italy*
[2] *German Research Center for Geosciences, Section 2.1, Telegrafenberg – 14473, Potsdam, Germany*
[3] *Dipartimento di Ingegneria Civile Edile e Ambientale, Sapienza – Università di Roma, Via Eudossiana, 18 – 00148, Rome, Italy*
e-mail: *brizzi.silvia@gmail.com*
session: *(Seismo-) Tectonics*

The majority of global seismicity originates at subduction zones, both within the converging plates and along the plate interface. In particular, most of the events with Mw > 8.0 (usually known as mega-earthquakes) occurs along the subduction thrust fault, i. e., the frictional interface between the subducting and overriding plates. Consequently, subduction zones generate Earth's largest earthquakes and most destructive tsunamis, being responsible for about 90 % of the seismic moment globally released during the last century [e. g., Pachecho & Skyes, 1992]. Contrary to popular belief, mega-earthquakes are not rare events. Indeed, numerous megathrust events have occurred at subduction zones during the last decade, often revealing unexpected characteristics. As tragically demonstrated by 2011 Tohoku, 2008 Maule and 2004 Sumatra earthquakes, these events often impact densely populated coastal areas and cause large numbers of fatalities and damages to infrastructures.

Understanding mega-earthquakes behaviour is particularly challenging. While scientists have a general comprehension of the subduction thrust fault seismogenesis, its physics still remains poorly constrained. This is mainly due to the short (i. e., limited to the past century) instrumental seismic history, which does not provide enough temporal perspective on the recurrence time of these big events and can be misinterpreted using oversimplifying assumptions. Moreover, except for discrete and punctual observations (e. g., Japan Trench Fast Drilling Project) what is known about subduction thrust fault behaviour derive from indirect methodologies, such as InSAR deformation measurements, land geodetic data and geophysical studies of convergent margins. Over time, scientific community made great efforts to gain a better physical understanding of subduction seismic cycle, because this would have fundamental implications on seismic hazard assessment of convergent margins. In addition to the previously mentioned methodologies, numerical [e. g., Wang, 2007; Kaneko et al., 2010; van Dinther et al., 2013] and analogue modelling [e. g., Rosenau et al., 2009; 2010; Corbi et al., 2013] can also be used as key-tool to study subduction earthquake cycle. In particular, analogue models have been widely used to investigate processes related to small-scale/short-term and large-scale/long-term earthquake physics, because of the great advantage of overcoming the restricted direct observation in space and time related to subduction thrust fault behaviour. Moreover, with the advent of deformation monitoring techniques, analogue modelling has entered the stage of becoming a potentially quantitative method.

First properly scaled analogue experiments with realistic geometries (i. e., wedge-shaped) suitable for studying interplate seismicity have been realized using granular elasto-plastic [e. g., Rosenau et al., 2009] and viscoelastic materials [e. g., Corbi et al., 2013]. Viscoelastic laboratory experiments consist of a type A 2.5 wt.-% gelatin wedge, under-thrusted by a rigid steel conveyor plate (i. e., the analogue of subducting plate), with defined velocity-weakening and –strengthening regions. Type A gelatin is an innovative analogue material that has: a) proper rheological properties to simulate downscaled lithospheric rock behaviour [Di Giuseppe et al., 2009] and b) appropriate transparency, that allows non-intrusive and continuous monitoring of the evolution of the model. This new geodynamical approach simulates the basic physics governing the subduction seismic cycle and related rupture processes, in a simplified yet robust way, helping to contribute to our understanding of mega-earthquakes. Despite the strength of the methodology, analogue earthquakes are not perfectly comparable with natural observations, especially in terms of recurrence time, coseismic duration and slip. The aim of this study is, therefore, to improve subduction seismic cycle analogue models, implementing: a) rheological properties of the analogue material and b) images analysis technique adopted for the experimental monitoring. In particular, this has been achieved with subsequent steps schematically illustrated in fig. 1.

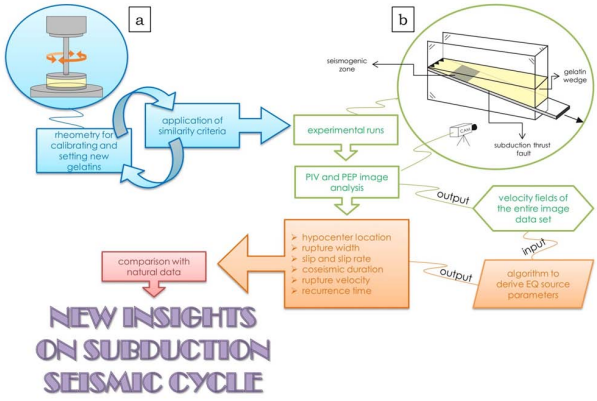

Fig. 1.: Workflow describing the main steps of the project; a) schematic drawing of parallel-plate rheometer used to determine the rheological properties of gelatin samples; b) schematic drawing of the experimental apparatus.

Although type A 2.5 wt% gelatin is the analogue material that best approximate lithospheric viscoelastic behaviour under laboratory conditions, in this work we aim at improving pre-existing experimental scaling factors. In order to quantify and compare periodicity and source parameters of analogue earthquakes as a function of lithospheric rheology, we use type A gelatin with greater concentration (i. e., 3 wt.-% and 6 wt.-%). The selection of new analogue materials, properly scaled with rheological viscoelastic behaviour of the lithosphere, has been realized with the approach commonly used in Material Science, i. e., measuring the deformation energy stored in the sample during the shear process and lost afterwards [e. g., Mezger, 2002]. The results of this work show that elastic and viscous properties of the analogue materials play important role in controlling seismogenic behaviour of subduction thrust fault, improving similarities with natural mega-earthquakes.

Models realized in this study have also been implemented in terms of monitoring system. In particular, model deformation has been derived by means of PEP (ParticlE and Prediction velocity) algorithm, belonging to PTV (Particle Tracking Velocimetry) techniques. Similarly to the usually adopted PIV (Particle Image Velocimetry) technique, PEP is an optical method used for extracting velocity field in fluid flows via the reconstruction of tracer particles seeding the media under investigation [e. g., Shindler et al., 2012]. PEP differs from classic cross-correlation techniques (i. e., PIV) in its ability to provide sparse velocity vectors at points coincident with particle barycentre positions. Velocity field is then evaluated from a Lagrangian point of view, allowing a larger spatial resolution (in the order of sub-pixel dimensions) compared to PIV. Outputs of PEP algorithm (i. e., velocity field of the images data set acquired during the experiments) are post-

processed using an ad hoc algorithm in order to obtain a set of seismologically relevant parameters, i. e., earthquake source parameters. In order to verify the implementation of monitoring system, experiments have also been analysed by means of PIV method, accordingly to Corbi et al. [2013]. Earthquake source parameters derived by PEP and PIV algorithm have also been compared in order to detect possible differences between the two methodologies. Preliminary results show that PEP algorithm is able to identify a greater number of analogue earthquakes, compared to PIV, detecting also smaller analogue earthquakes. Furthermore, spatio-temporal slip rate and cumulative slip distributions are defined with higher and sharper resolution in the space domain compared to PIV. PEP algorithm is then suitable to potentially gain new insights on seismogenic process of subduction thrust fault. Moreover, the ability to distinguish analogue earthquakes of different sizes may also have implications on successful applicability of scaling relationship, such as Gutenberg-Richter law, to experimental results.

References

Corbi, F., F. Funiciello, M. Moroni, Y. van Dinther, P. M. Mai, L. A. Dalguer & C. Faccenna (2013) – The seismic cycle at subduction thrusts: 1. Insights from laboratory models. J. Geophys. Res. Solid Earth, 118, 1483-1501, doi:10.1029/2012JB009481

Di Giuseppe, E., F. Funiciello, F. Corbi, G. Ranalli & G. Mojoli (2009) – Gelatins as rock analogs: A systematic study of their rheological and physical properties. Tectonophysics, 473(3-4), 391–403, doi:10.1016/j. tecto.2009.03.012.

Kaneko, Y., J.-P. Avouac & N. Lapusta (2010) – Towards inferring earthquake patterns from geodetic observations of interseismic coupling. Nat. Geosci., 3(5), 363–369, doi:10.1038/ngeo843

Pacheco, J. F. & L. R. Sykes (1992) – Seismic moment catalog of large shallow earthquakes, 1900 to 1989. Bull. Seismol. Soc. Am., 82, 1306–1349.

Rosenau, M., J. Lohrmann & O. Oncken (2009) – Shocks in a box: An analogue model of subduction earthquake cycles with application to seismotectonic forearc evolution. J. Geophys. Res., 114(B1), 1–20, doi:10.1029/2008JB005665.

Rosenau, M., R. Nerlich, S. Brune & O. Oncken (2010) – Experimental insights into the scaling and variability of local tsunamis triggered by giant subduction megathrust earthquakes. J. Geophys. Res., 115(B9), 1–20, doi:10.1029/2009JB007100.

Shindler, L., M. Moroni & A. Cenedese (2012) – Using optical flow equation for particle detection and velocity prediction in particle tracking. Applied Mathematics and Computation, 218, 8684–8694, doi:10.1016/j.amc.2012.02.030.

van Dinther, Y., T. V. Gerya, L. A. Dalguer, F. Corbi, F. Funiciello, & P. M. Mai (2013) – The seismic cycle at subduction thrusts: 2. Dynamic implications of geodynamic simulations validated with laboratory models. J. Geophys. Res. Solid Earth, 118, 15021525, doi:10.1029/2012JB009479.

Wang, K. (2007) – Elastic and viscoelastic models of crustal deformation in subduction earthquake cycles, in The Seismogenic Zone of Subduction Thrust Faults, MARGINS Theoretical and Experimental Earth Science Series, edited by T. H. Dixon & J. C. Moore, Columbia Univ. Press, New York.

Upscaling of micro- and meso-scale structures to local- and regional scales: implications for 3D implicit and explicit models of structurally complex deformation of multi-layered rocks

Mathias Egglseder[1], Alexander Cruden[1]

[1]*School of Geosciences, Monash University, Melbourne, Victoria 3800, Australia*
e-mail: *mathias.egglseder@monash.edu*
session: *(Seismo-) Tectonics*

An ideal geological model should account for all structures from the micro- to the regional scale using the principle that small-scale structures can be extrapolated to larger-scale structures and vice-versa. In reality, this task is not straightforward if the structural evolution of an area is complicated by overprinting ductile and brittle deformation events and contrasting rheological behaviors of rock types. In order to address this practical challenge, we will evaluate whether insights provided from micro- and meso-scale structures observed in thin sections and hand specimens can be upscaled to the geometry and spatial-timing relationships at a larger local to regional scale. Our approach is to visualize complexly-deformed hand specimens using explicit (Move, Midland Valley Ltd.) modelling techniques to characterize the 3D geometry of relevant structural features, supported by microstructural observations. The results are then compared with structural observations in outcrops and 3D mine-scale models using implicit (Leapfrog, AranzGeo Ltd.) modelling techniques, which offer spatial information on a larger scale.

The 3D deformation of multilayered rocks with different rheological properties has been studied using analogue and numerical modelling, but results to date have been difficult to apply to complex geologic settings. A complementary approach to improve understanding of the complex 3D deformation of multilayered rocks is to carry out 3D multiscale analysis and geometric modelling in a field area containing contrasting lithologies that has been affected by multiple deformation phases. These requirements are prevalent in deformed Neoarchean to Paleoproterozoic banded iron formations (BIF) of the Hamersley Province, Australia. Here, sedimentary rocks comprise mm to dm thick bands of alternating chert and iron oxide layers, interbedded with shales, carbonates and volcanic rocks. The stratigraphic succession is laterally consistent with no significant facies changes over large distances (Morris 1993), making the BIFs an ideal laboratory to study the deformation of multilayers with different rheological behaviors in three dimensions. The area is also well exposed and extensive subsurface data is available due to iron ore mining operations and exploration activities. Here we take advantage of 50 years of data acquisition by Rio Tinto Ltd. at the Mount Tom Price mine to create a 3D model of the deposit in order to characterize the 3D geometry of a key part of this structurally complex region. The rock units experienced several proposed shortening and extensional deformation stages with an only low grade metamorphic overprint (e. g. Taylor et al. 2001; Müller et al. 2005; Dalstra 2006; Morris & Kneeshaw 2011).

Our new structural approach attempts to challenge the many debated aspects of BIF formation, the structural evolution of the region and the enrichment processes that lead to BIF-hosted

Fig. 1.: Thin chert layers in shale show different deformation compared to thick overlying BIF layers.

Fig. 2.: Complex structural features of chert layers (red) in shales (black).

high-grade iron ore deposits. Different analysis techniques have been used to approach these topics incorporating basic field mapping and microscopy, 3D visualization using X-ray microscopy (XRM) and 3D modelling techniques to develop 3D models on all scales. Field observations indicate complex relationships between structural features, with simultaneous formation of brittle and ductile structures controlled by the rheological properties of the different rock units (Fig. 1 and Fig. 2). Folds are commonly non-cylindrical and faults die out rapidly vertically and horizontally, creating challenges for the recognition of overprinting relationships.

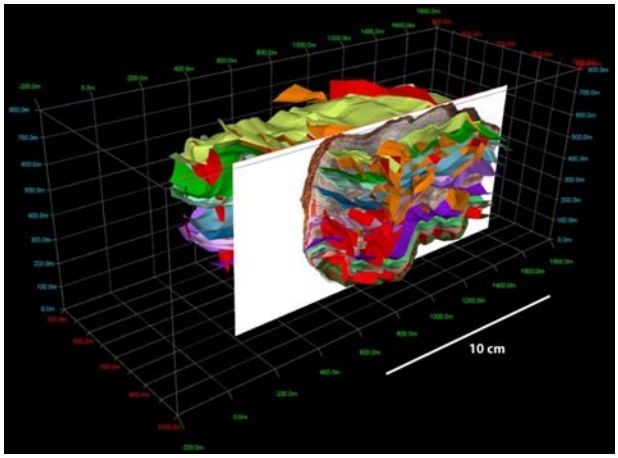

Fig. 3.: 3D Move (by Midland Valley Ltd.) model of complexly deformed specimen

In order to better resolve these structural relationships, serial sections of a complexly deformed hand specimen of BIF were digitized and then used to create an explicit 3D model with 3DMove (Midland Valley Ltd.) (Fig. 3). The model shows that structural features are controlled by differences in the rheological properties of chert and iron oxide layers, which has led to complex deformation patterns at all scales. The resulting structural analysis shows at least two deformation events. A first extensional event (D 1) led to the development of pinch-and-swell structures and boudinage of more competent cherty layers. A later (possibly two-stage) shortening event (D 2) is indicated by buckling, mullion structures and thrusting, which are mainly controlled by the rheological contrasts between rock units (Fig. 4).

Microscopic studies (optical and XRM) indicate significant removal of quartz, which leads to a reduction of layer thicknesses and hence a compacted sequence of iron oxides (Fig. 5) alongside reprecipitation as fibrous strain fringes (Passchier & Trouw 2005) in extensional domains associated with martite-crystals (martite: pseudomorph of hematite after magnetite). A cleavage also developed in the flattening plane and is indicated by a second generation of iron oxides precipitated by iron-rich fluids.

Similar structural features arising from rheological contrasts between chert, iron oxides and

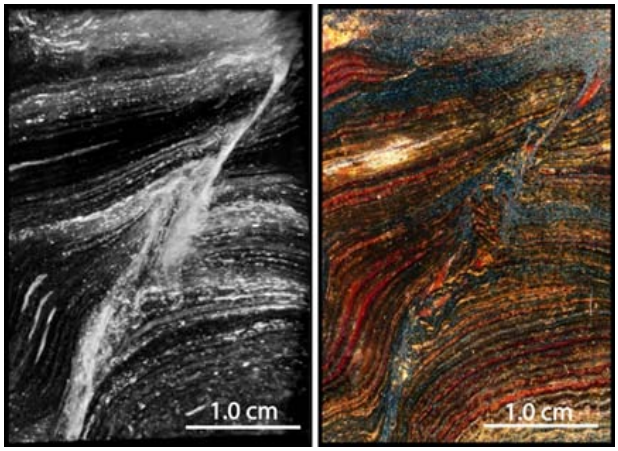

Fig. 4.: Complex structures compared; left: XRM image, right: photo scan

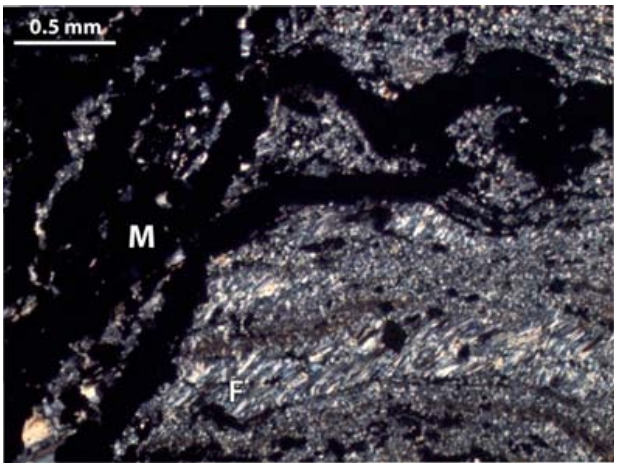

Fig. 5.: Dissolution of quartz leads to reduced iron oxide layers and reprecipitation as fibrous strain fringes (F), M: Martite

shales are also observed in outcrops and in deposit scale models (Fig. 6). Contrasting fluid flow properties between lithologies (e. g. BIF and shales) may also have played a major role leading to different styles of deformation and the development of a variety of fold and fault geometries (e. g., Marques et al. 2010).

The extrapolation of these smaller scale structures to larger scales using 3D modelling techniques depends on the complexity of the geology and the data available (Calcagno et al. 2008). To generate a 3D model of the Mount Tom Price mine (Fig. 7) we have used the implicit modelling

Fig. 6.: Complex relationships between boudins, folds and faults due to different rheological behaviour

software Leapfrog (AranzGeo Ltd.), which interpolates raw datasets of numeric and non-numeric data (e. g., lithological boundaries, geochemical, geophysical, mapping and structural data) using a single mathematical volume function (RBF: radial basis function) into a single coherent model. In contrast, the alternative explicit modelling techniques introduce inherent bias because models are typically built from already interpreted 2D cross-sections. The advantage of implicit modelling is that the interpolation process is relatively unbiased. However, it requires a consistently high data density and does not produce satisfactory results away from data points (see Fig. 7, isosurfaces are not well constrained at certain distances to the drill hole data) and is therefore not yet utilizable in the same resolution for regional scale models with fewer data points (no drill hole data).

Figure 7 shows a cross section through the main part of the Mount Tom Price iron ore deposit with the least amount of user-defined interpretation. The main structure is a major syncline with a SW-dipping normal fault on its NE limb, which appears to exploit shale layers as detachment horizons. In 3D and at the local and mine scale, the trends of this and other faults are often not clear, which could be explained by contrasts in rheological behaviour between shale- and BIF units. Relative large distances between exploration drill holes often do not permit observation

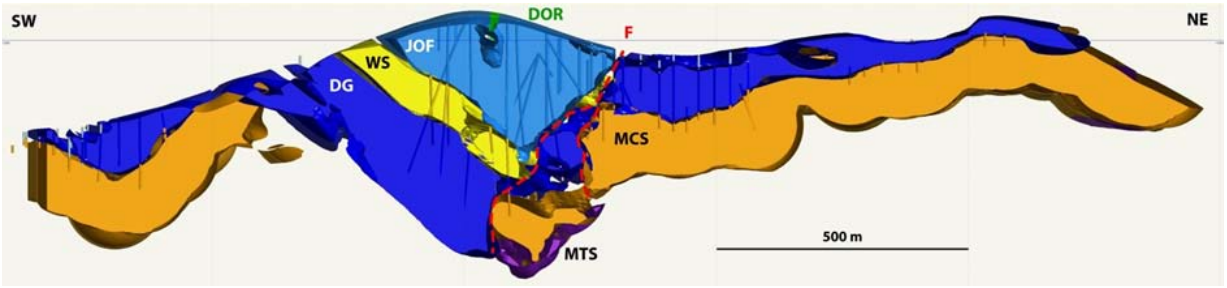

Fig. 7.: Cross section of the 3D Leapfrog model. Holes are subject to the distance to data points of drill holes. DOR: Dolerite, F: Fault, JOF: Joffre Mb. (BIF), MCS: Mt. McRae Shale, MTS: Mt. Sylvia Fm. (Shale/chert), WS: Whaleback Shale Member

of smaller scale structures.

Our preliminary analysis shows that similar structures can be observed on smaller and larger scales, e. g., thickness variations and the absence of individual layers due to extensional and compressional deformation, non-cylindrical and converging folds as well as vertically and horizontally discontinuous faults. Different lithologies are variably affected by synchronous folding and faulting and by simultaneous dissolution and reprecipitation on a microscale. These complimentary observations suggest that similar mechanisms of deformation are prevalent on all scales, which is an implication that would have arisen without extensive study of smaller scale structures.

We hypothesize that the above structural associations established a framework for later enrichments and replacements that led to the formation of high-grade iron ore. Since the 3D deformation of multilayers with contrasting thickness and lithology is not well understood, our approach also provides insights on the variable behaviors of different rock units on all scales. 3D analysis of the resulting structures at the meso-scale and their subsequent extrapolation to larger scales is an effective way to significantly improve the understanding of complex structural processes. Although 3D modelling tools are important and helpful for this analysis they cannot replace basic structural geology combined with different fields of geology (here: petrography, microtectonics, geochemistry). Consideration of all available geological data is crucial to create a realistic geological model, which is able to explain all observable features for academic as well as applied purposes.

References

Calcagno, P., Chilès, J.P., Courrioux, G., Guillen, A., 2008. Geological modelling from field data and geological knowledge. Physics of the Earth and Planetary Interiors, 171(1-4), 147–157.

Dalstra, H.J., 2006. Structural controls of bedded iron ore in the Hamersley Province, Western Australia – an example from the Paraburdoo Ranges. Applied Earth Science: IMM Transactions section B, 115(4), 139–145.

Marques, F.O., Burg, J.-P., Lechmann, S.M., Schmalholz, S.M., 2010. Fluid-assisted particulate flow of turbidites at very low temperature: A key to tight folding in a submarine Variscan foreland basin of SW Europe. Tectonics, 29(2), TC2005, doi:10.1029/2008TC002439.

Morris, R.C., 1993. Genetic modelling for banded iron-formation of the Hamersley Group, Pilbara Craton, Western Australia. Precambrian Research, 60, 243–286.

Morris, R.C. & Kneeshaw, M., 2011. Genesis modelling for the Hamersley BIF-hosted iron ores of Western Australia: a critical review. Australian Journal of Earth Sciences, 58(5), 417–451.

Müller, S.G., Krapež, B., Barley, M.E., Fletcher, I.R., 2005. Giant iron-ore deposits of the

Hamersley province related to the breakup of Paleoproterozoic Australia: New insights from in situ SHRIMP dating of baddeleyite from mafic intrusions. Geology, 33(7), 577-580.

Passchier, C.W. & Trouw, R.A.J., 2005. Microtectonics. 2nd edition, Springer Verlag, Berlin, Heidelberg, 366pp.

Taylor, D., Dalstra, H.J., Harding, A.E., Broadbent, G.C., Barley, M.E., 2001. Genesis of High-Grade Hematite Orebodies of the Hamersley Province, Western Australia. Economic Geology, 96, 837–873.

Influence of the seismogenic downdip width on supercycles at subduction thrusts

Robert Herrendörfer[1], Ylona van Dinther[1], Taras Gerya[1], Luis A. Dalguer[1,2]

[1]*ETH Zurich, Institute of Geophysics*
[2]*now at swissnuclear*
e-mail: *robert.herrendoerfer@erdw.ethz.ch*
session: *(Seismo-) Tectonics*

Introduction

Megathrust earthquakes exhibit a strong variability in size and extent both in strike and dip direction. For instance, in the north-east Japan subduction zone mainly M 7 earthquakes had ruptured a small part of the rupture area of the 2011 M 9.0 Tohoku earthquake that appears to have spanned the entire seismogenic zone downdip width [e. g. 5]. In some of the cases when a long record of past earthquakes is available, a recurring earthquake pattern seems to arise, which is called supercycle [1, 2]. It contains the occurrence of smaller earthquakes in between larger earthquakes. A better understanding of this variability in earthquake size would contribute to an improved hazard assessment in areas close to subduction zones. We observe that supercycles have been proposed for those subduction zones [1,2] with a large seismogenic zone downdip width [3] (Fig. 1), including the north-east Japan subduction zone. This suggests a potential role of the downdip width. In this numerical study we show that the downdip width is indeed the key parameter controlling the long-term seismicity at subduction thrusts.

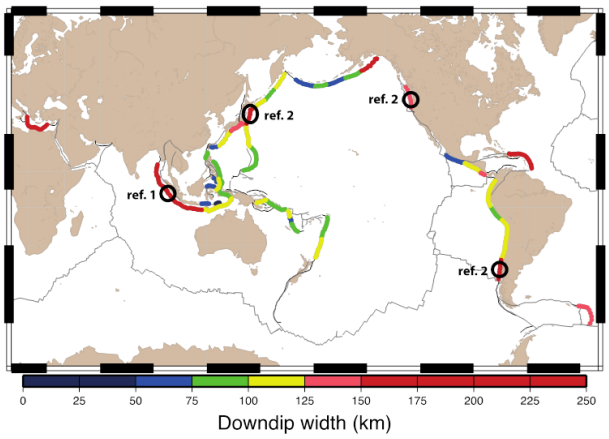

Fig. 1.: Downdip width of seismogenic zones and proposed supercycles. Supercycles have been proposed [1, 2] for seismogenic zones with an estimated wide downdip width [3]. Adapted from [3]. Colorscale corresponds to the distributionof the downdip widths, with red colors indicating subduction zones outside one standard deviation from the mean value.

Methods

To investigate the role of the seismogenic downdip width, we use a two-dimensional continuum, seismo-mechanical numerical model of a simplified subduction zone [4]. Under the assumption

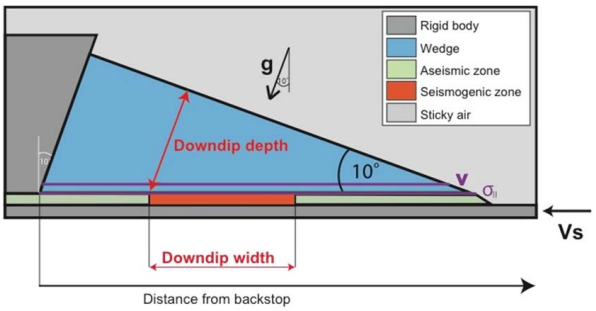

Fig. 2.: Numerical model setup. A visco-elastic wedge is underthrusted by a rigid plate with a subduction velocity of Vs and at a subduction angle of 10°. The interface between the wedge and the plate is modeled as a frictional boundary layer. In this layer, the seismogenic zone, modelled as velocity-weakening, is limited up- and downdip by aseismic zones, modelled as velocity strengthening. Horizontal displacement velocity is measured 1 cm above, stress and strength at the top of the frictional boundary layer.

of an incompressible medium, we solve for the conservation of mass and momentum and apply a visco-elasto-plastic rheology. The model setup (Fig. 2) consists of a visco-elastic wedge that is underthrusted by a rigid plate. In the frictional boundary layer between plate and wedge, we apply a pressure-dependent yield strength, a non-associative plastic flow law and a strongly rate-dependent friction. In this layer, a velocity-weakening seismogenic zone is limited up- and downdip by velocity-strengthening aseismic areas. Here, model results and parameters are scaled up to natural values. Main model limitations include the restriction to 2D, a non-adaptive time-step, and negligible wave propagation effects.

We compare different models using functions and parameters, averaged over the width of the seismogenic zone: cumulative sum of displacements tracks the evolution of elastic strain, strength excess depicts the stress state and the S parameter is the ratio of initial strength excess and stress change for each event. Furthermore, we calculate the average supercycle duration and the average number of events per supercycle. We qualitatively distinguish between sub-critical, pulse-like and crack-like ruptures by evaluating the propagation distance, local duration of coseismic displacements and the existence of healing during an event.

Results

In the reference model with a downdip width of 248 km (LW) supercycles evolve (Fig. 3 a). Interseismic deformation concentrated at the seismogenic zone limits, small sub-critical and pulse-like ruptures effectively increase the stress within the seismogenic zone to a critical state (Fig. 3 b-c). A supercycle is then completed by a large crack-like rupture (i. e. superevent), which strongly reduces stresses in the entire seismogenic zone. A model with a downdip width of 102 km (SW), in contrast, is characterized by ordinary cycles, mainly consisting of similar sized, quasi-periodical crack-like ruptures (Fig. 3). Increasing the seismogenic zone downdip width thus leads to a transition from ordinary cycles to supercycles as the number and variability of events increase (Fig. 4 a) as well as the size of and recurrence time between the largest events. It also leads to an increase of the median S parameter, indicating a transition from the dominance of crack-like ruptures to the dominance of pulse-like ruptures (Fig. 4 b).

Other factors which can be shown with our model to influence supercycles are 1) downdip depth of the seismogenic zone, 2) a large strength excess due to a relatively strong megathrust and 3) large stress drops due to a strongly rate-dependent friction.

With our 2D model we cannot rule out the hypothesis that the observation of supercycles might be a result of strength or frictional heterogeneities along the dip and strike of the megathrust or due to earthquake interactions from different segments.

Conclusions

In the reference model with a downdip width of 248 km (LW) supercycles evolve (Fig. 3 a). Interseismic deformation concentrated at the seismogenic zone limits, small sub-critical and pulse-like ruptures effectively increase the stress within the

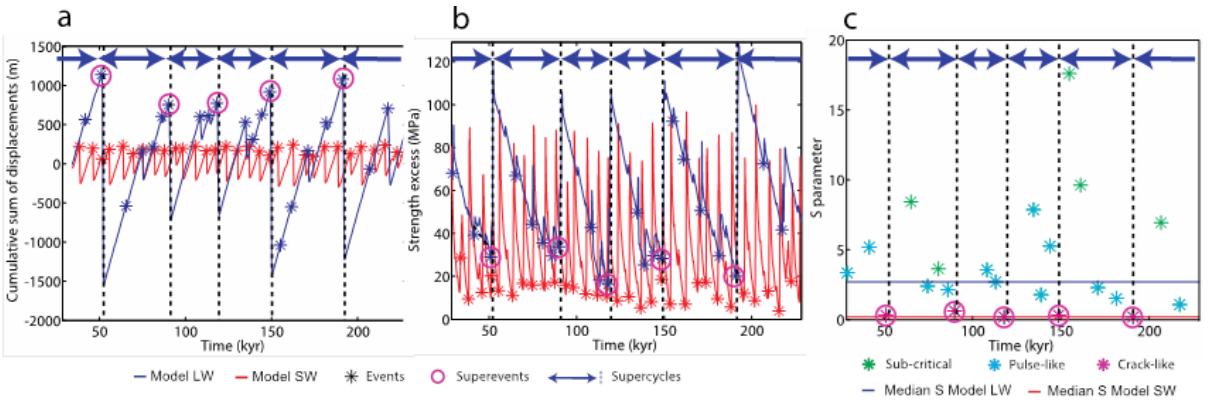

Fig. 3.: Results for reference models LW and SW. Functions and parameters, averaged over the downdip width of the respective seismogenic zone for model LW (downdip width=$248\,\mathrm{km}$) and for model SW (downdip width=$102\,\mathrm{km}$): a, Detrended, cumulative sum of displacements over time, b, evolution of strength excess (i.e. difference between yield strength and second invariant of deviatoric stress tensor), c, S parameter (ratio between initial strength excess and stress change) over time in model LW, while colors of each event indicate the rupture style. Horizontal lines show the median S value for model LW and model SW. Stars represent detected events. Purple circles show superevents. Blue arrows indicate the duration of supercycles in model LW.

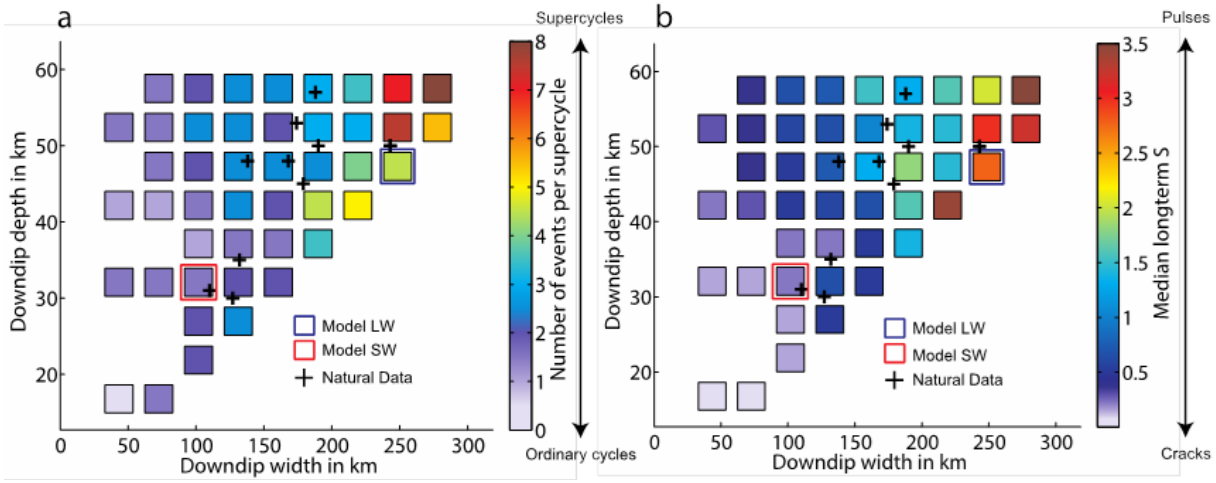

Fig. 4.: Results of the parameter study. Role of the downdip width and depth of theseismogenic zone for a, the number of events and, b, the median of the S parameter. Model LW and SW are highlighted with blue and red squares, respectively. Black crosses indicate natural seismogenic zones, determined by [3]. The increase of the number of events indicates the transition from simple cycles to supercycles, while the increase of the median S paramater indicates the transition from the dominance of cracks to pulse-like ruptures.

seismogenic zone to a critical state (Fig. 3 b-c). A supercycle is then completed by a large crack-like rupture (i. e. superevent), which strongly reduces stresses in the entire seismogenic zone. A model with a downdip width of 102 km (SW), in contrast, is characterized by ordinary cycles, mainly consisting of similar sized, quasi-periodical crack-like ruptures (Fig. 3). Increasing the seismogenic zone downdip width thus leads to a transition from ordinary cycles to supercycles as the number and variability of events increase (Fig. 4 a) as well as the size of and recurrence time between the largest events. It also leads to an increase of the median S parameter, indicating a transition from the dominance of crack-like ruptures to the dominance of pulse-like ruptures (Fig. 4 b).

Other factors which can be shown with our model to influence supercycles are 1) downdip depth of the seismogenic zone, 2) a large strength excess due to a relatively strong megathrust and 3) large stress drops due to a strongly rate-dependent friction.

With our 2D model we cannot rule out the hypothesis that the observation of supercycles might be a result of strength or frictional heterogeneities along the dip and strike of the megathrust or due to earthquake interactions from different segments.

References

[1] Sieh et al. Earthquake Supercycles Inferred from Sea-Level Changes Recorded in the Corals of West Sumatra. Science, 322(5908):1674-1678, 2008.

[2] Goldfinger et al. Superquakes and Supercycles. Seismological Research Letters, 84(1): 24-32, 2013.

[3] Heuret et al. Physical characteristics of subduction interface type seismogenic zones revisited. G3, 12(1), Q01004, 2011.

[4] van Dinther et al.The seismic cycle at subduction zone thrusts: 2. Dynamic implications of geodynamic simulations validated with laboratory models. J. Geophys. Res., 118:1502-1525, 2013.

[5] Simons et al. The 2011 Magnitude 9.0 Tohoku-Oki Earthquake: Mosaicking the Megathrust from Seconds to Centuries, Science, 332 (6036), 1421-1425 2011

Geomechanical modeling of fault geometry role on subduction earthquake cycle: Case study of Chilean margin

Shaoyang Li[1], Marcos Moreno[1], Jon Bedford[1], Matthias Rosenau[1], Daniel Melnick[2], Onno Oncken[1]

[1] *Helmholtz Centre Potsdam, GFZ German Research Centre for Geosciences, Telegrafenberg, Potsdam, Germany*
[2] *Institut für Erd- und Umweltwissenschaften, DFG-Leibniz Center for Surface Process and Climate Studies, Universität Potsdam, Potsdam, Germany*
e-mail: *shaoy@gfz-potsdam.de*
session: *(Seismo-) Tectonics*

Introduction

Understanding the mechanical processes governing magnitude, recurrence, and segmentation of earthquakes along a subduction margin is of paramount importance for assessing the margin's seismic hazard. Long-term variations in fault friction and geometrical undulations of the plate interface are thought to be the first order controls on system behavior and activation. Many studies from analogue and numerical modeling have quantitatively investigated the effects of fault heterogeneities on earthquake cycle behavior [1], but a clear understanding of main controlling parameters remain elusive. An observable permanent/plastic strain is built up over multiple seismic cycles, producing geological features such as terraces and peninsulas [2] providing some constraints for the models. Co-, post- and interseismic kinematics of a margin are likely to be mainly an expression of the frictional properties controlling the stick-slip behavior of the plate interface and relaxation phenomena in the mantle wedge and deeper viscoelastic portion of the subduction zone lithosphere. Challenges remain in separating the contributions of these overlapping relaxation phases and interface kinematic processes in the data.

Short-term heterogeneous coseismic slip distribution on faults may be due to heterogeneous pre-stress, geometric complexity, heterogeneous material properties, dynamic weakening mechanism [3-5]. Recent studies of the dynamic modeling of geometric effects, such as fault bending, fault stepover, fault roughness, and parallel offset of faults, on rupture propagation (e. g. [5-8]) indicate that rupture tends to decelerate or terminate at places where the fault geometry varies. Some of these studies emphasize the importance of initial stress but normally with pre-defined unrealistic stress field or principle stress orientation, which may not represent tectonic loading due to geometric complexity in detail or any frictional heterogeneity. Moreover, initial stress can largely affect the seismic rupture and the ability of breaking past kinks or branches in the fault system [5, 7, 9]. Therefore, fault geometry and structure can heavily affect interseismic stress accumulation along fault system as well as the stress released in large ruptures.

Modern precise geophysical measurements give reasonable constrains on fault geometry, material properties and kinematics. Furthermore, decades of space geodetic observations are allowing to accurately quantify transient deformation associated with the earthquake cycle process [10-12]. These kinematic observations offer an excellent chance to model how large plate boundary fault system is evolving with unprecedented precision. Integrating geophysical and geodetic data with

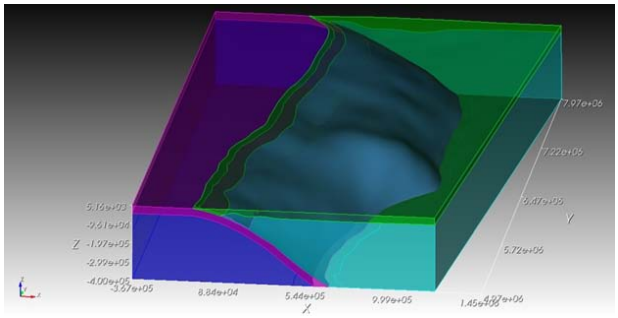

Fig. 1.: Geometry of whole Chilean subduction zone

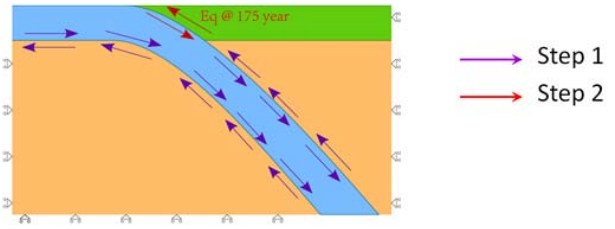

Fig. 2.: Two-step method of earthquake cycle modeling

numerical modeling shade some lights on mechanisms of earthquake cycle of large plate boundary fault system establishing new tools that were not available. In this context, we attempt to evaluate geometry effects on the earthquake cycle (without considering permanent friction heterogeneity [1]) using the Finite Element Method (FEM) (Figure 1) and all available geophysical and geodetic data for the entire Chilean interplate margin. We simulate an earthquake cycle to investigate the continuous complex geometry effects on pre-seismic stress heterogeneities, dynamic strong-holder-breaking rupturing, and long-term earthquake segmentations, hence long-term fault system seismic hazards. Our study emphasizes the importance of considering the geometrical complexity during all phases of the earthquake cycle.

Method

We construct a FEM including precisely all the geomechanical heterogeneities of the Chilean subduction zone (Figure 1) [13, 14]. Our models attempt to quantify the control of geometrical features on the buildup of high shear stress along a fault and their direct mechanical on seismic barrier or asperities. Therefore, we implemented a simple method with two forward steps: Firstly, we simulate tectonic loading of interseismic period with complex realistic geometry and geodetically derived plate convergence and forearc deformation. Here, we imposed a homogenous locking degree along the fault, and therefore only the geometrical features control lateral variations of strain accumulation. Secondly, we mimic a coseismic rupture releasing the interseismic accumulated stress in first step (shown as Figure 2). Hence our modeling emphasizes the importance of producing realistic pre-stress on a dynamic model, task that is not well described on literature.

Preliminary results

We successfully produce rough segmentations along whole Chilean subduction zone in our preliminary test of our model set up (Figure 3 b). Comparing to the nature earthquake history, we find out our model well reproduce large segmentation in south Chile where 1960 M_w 9.5 earthquake happens. However, our model cannot reproduce all details along the margin. This may due to inaccurate interseismic kinematics and the variation in reoccurrence period for different segments.

Future work

We plan to add complexity in both interseismic and coseismic model. By simulating gravity stresses as background stress, we can better constrain fault opening during coseismic simulations. Better interseismic models may involve realistic loading (variation of convergence along the trench) and reliable geodetic inverted locking degrees in seismogenic zones. Using dynamic method (i. e. explicit scheme of finite element method), our model can better catch the characters of megathrust earthquake rupturing, which result in subduction zone segmentations. We will calculate the distribution of locking and attempt to include the influence of the Andean Shortening

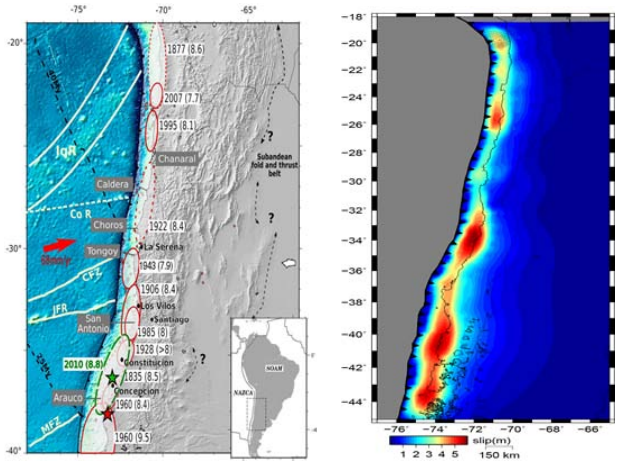

Fig. 3.: Comparison of surface deformation of our model with historical segmentation along whole Chilean margin. (a) Historical megathrust earthquakes segmentation [15]. [2] Preliminary result of surface deformation from our simple earthquake cycle model of geometry complex.

on the GPS signals. In this way, we will archive better final solution to compare the locking degree of short term crystal deformation based on GPS observations with the asperities and barrier patchwork from the stress release.

References

[1] Y. Kaneko, J. P. Avouac, N. Lapusta, Nature Geosci. 3, 363 (2010).

[2] D. Melnick, B. Bookhagen, H. P. Echtler, M. R. Strecker, Geological Society of America Bulletin 118, 1463 (November 1, 2006, 2006).

[3] C. H. Scholz, Nature 391, 37 (1998).

[4] P. M. Mai, G. C. Beroza, Journal of Geophysical Research-Solid Earth 107, (Nov, 2002).

[5] B. Duan, D. D. Oglesby, Journal of Geophysical Research: Solid Earth 111, B05309 (2006).

[6] Y. Kase, K. Kuge, Geophysical Journal International 135, 911 (December 1, 1998, 1998).

[7] B. Duan, D. D. Oglesby, BULLETIN OF THE SEISMOLOGICAL SOCIETY OF AMERICA 95, 1623 (2005).

[8] T. Candela, F. Renard, J. Schmittbuhl, M. Bouchon, E. E. Brodsky, Geophysical Journal International 187, 959 (2011).

[9] N. Kame, J. R. Rice, R. Dmowska, Journal of Geophysical Research: Solid Earth (1978–2012) 108, (2003).

[10] J. Klotz et al., Earth and Planetary Science Letters 193, 437 (2001).

[11] J. Bedford et al., Earth and Planetary Science Letters 383, 26 (2013).

[12] M. Moreno et al., Earth and Planetary Science Letters 321–322, 152 (2012).

[13] A. Tassara, H. J. Goetze, S. Schmidt, R. Hackney, J. Geophys. Res. 111, B09404 (2006).

[14] G. Hayes. (Nature Publishing Group, a division of Macmillan Publishers Limited. All Rights Reserved., 2010).

[15] M. Metois, A. Socquet, C. Vigny, J. Geophys. Res. 117, B03406 (2012).

The long term evolution of fold-and-thrust belts: consistency of numerical approaches and physical experiments

Bertrand Maillot

Laboratoire Géosciences et Environnement Cergy, Université de Cergy-Pontoise, France
e-mail: *bertrand.maillot@u-cergy.fr*
session: *(Seismo-) Tectonics*

The recent developments in numerical techniques to describe large slip on frictional surfaces and the formation of faults, have allowed us to simulate numerically the long term evolution of fold-and-thrust belts, which were so far only simulated with physical experiments. Therefore, the question of the fit between various numerical solutions (Buiter et al., 2006), and physical analogue experiments (Schreurs et al., 2006), has become central. This presentation will focus first on the production of experimental data that can be quantitatively compared to numerical simulations, and second on the development of a numerical method to simulate the experimental data and further used to predict the spatio-temporal activity of faults during the very long term growth of an accretionary wedge, thereby suggesting further experiments.

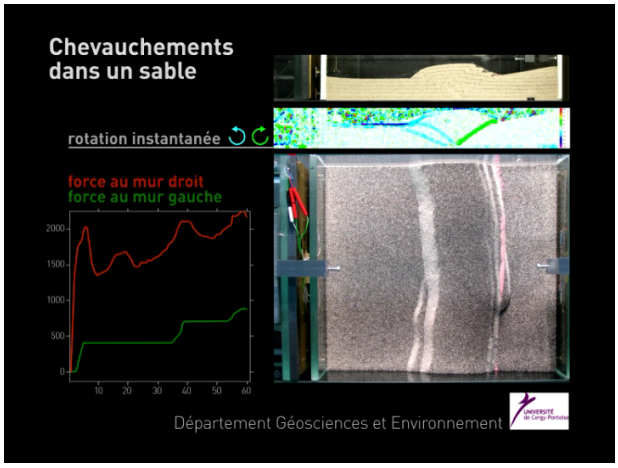

Fig. 1.: A typical thrusting experiment. Top right: lateral view through the glass side wall, with map of rotations below (obtained by PIV); bottom right: top view; bottom left: force measured at each end walls (red: right) during shortening (mm). (P. Souloumiac, PhD)

Experimental Data

Fig. 1 illustrates a basic thrusting experiment. Its simulation with a 2D numerical code raises a series of questions. Should the comparison be made with the side view, or with a cross-section in the center (that can be observed only post-mortem in the absence of a scanner)? What is the reproducibility of the experimental cross-section? How to measure quantitatively the fit of a simulation to a cross-section? These questions find general answers in the theory of inverse problems. I will present some of their specific aspects for a thrusting experiment using sand, among which the problem of building the sand pack, of side wall friction (Fig. 2), of force measurement, and a protocol to establish error bars that account for the lateral variability of thrusting.

Numerical approach by sequential limit analysis

Although numerical methods that solve the full mechanical problem (various FEM techniques), as well as DEM methods are rapidly progressing, the

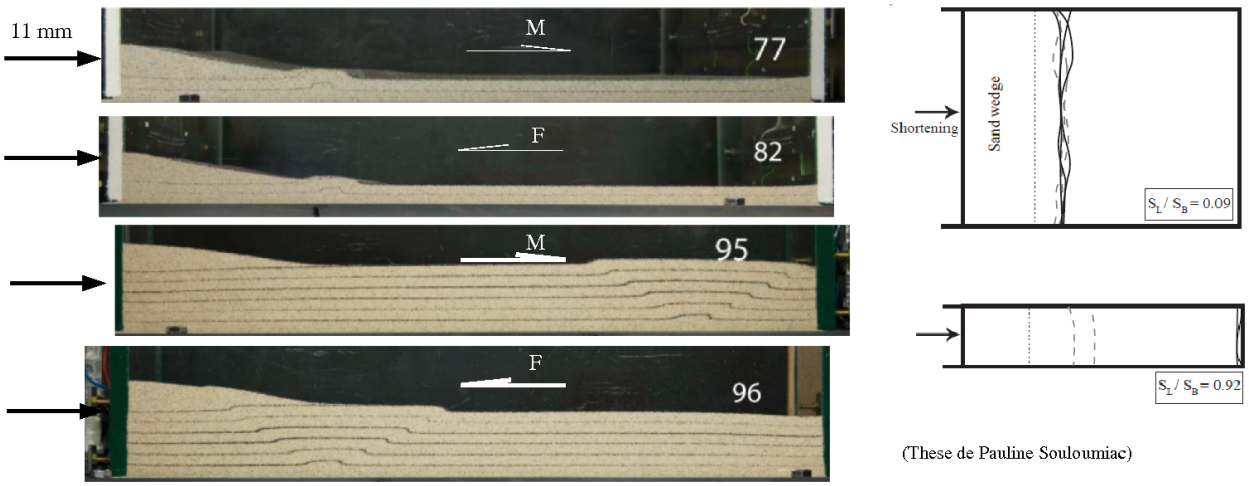

Fig. 2.: Illustration of side wall friction effects. M: mobile base configuration (equivalent to conveyor belt, or "pull" type of box); F: fixed base configuration (equivalent to boxes using a single moving wall, or "push" type). At low lateral to basal area ratio (SL/S_B), results are the same (top two photos), but at high SL/S_B values, thrusting occurs at opposite ends of the box (bottom two photos), demonstrating a strong bias. (P. Souloumiac, PhD)

kinematic approach of Limit Analysis, also called the maximum strength theorem (MST) (Maillot and Leroy, 2006), offers a simplified method to determine the active fault geometry accounting for mechanical balance and the Coulomb criterion (Cubas et al., 2008, Mary et al., 2013a, 2013b). Its sequential application leads to the Sequential Limit Analysis (SLA) method. I will briefly present the method and its ability to reproduce experiments (Fig. 3). The very long term growth by frontal accretion reveals a complex pattern of thrust ramp activity (called G-grams) grouped in families (Fig. 4). The introduction of ramp friction weakening, perturbs this pattern and creates periods of inactivity of ramps in the back of the wedge that were not previously documented. Current developments focus on gravitational instability in over-pressured materials (Yuan et al., 2014). Longer term developments will focus on a 3D implementation, and on varying material properties within the sedimentary pile.

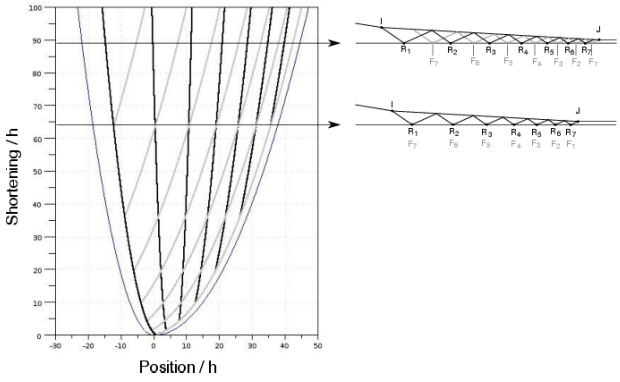

Fig. 4.: Spatio-temporal pattern of thrust ramp distribution (G-gram) during frontal accretion in a frictional wedge, showing "in phase" (at shortening=64) and "out-of-phase" periods (at shortening=89) between the families R and F of thrust ramps issued respectively from the deformation fronts at the back (point I) or the front (point J) of the wedge. (B. Mary, PhD).

Perspectives

Because SLA uses the same parameters as the Critical Coulomb Wedge theory, but provides the

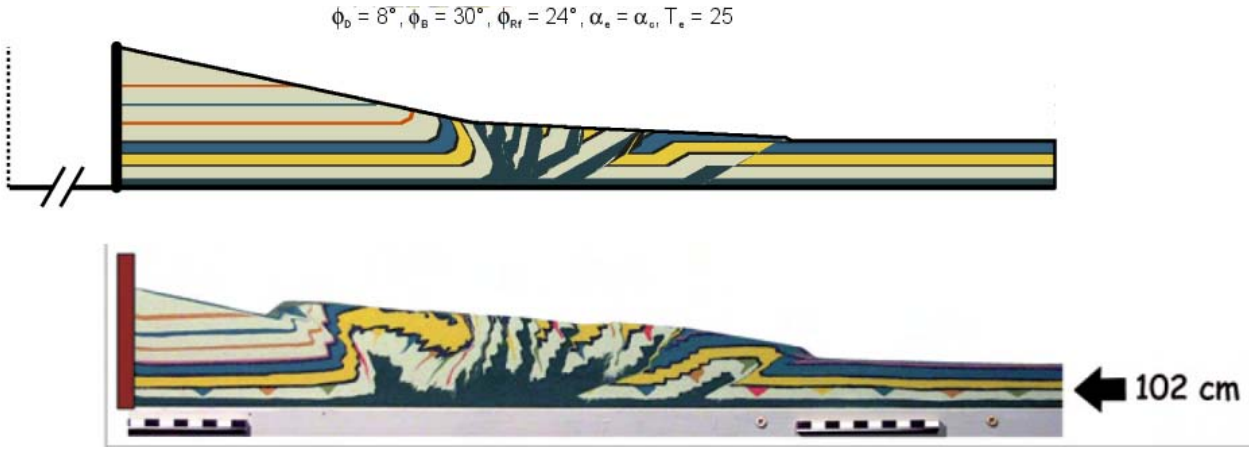

Fig. 3.: Comparison between a numerical simulation by Sequential Limit Analysis (SLAMTec), and a sand box experiment (Konstantinovskaya and Malavieille, 20xx) (B. Mary, PhD)

internal deformation during wedge growth, it can be seen as a generalisation of the CCW theory. Its predictions could be used as benchmarks for the more complex and general numerical methods, and suggest further experiments to compare to the spatio-temporal thrusting patterns mentioned above. Concerning experimental data, protocols to produce data with well defined statistical properties for comparison with 3D numerical simulations should now be developed, inspired by the 2D procedure. Overall, the comparison of experimental and numerical data in the framework of inverse problem theory, although not yet accessible for most numerical methods, is a very demanding and fruitful objective. It helps us to raise levels of both approaches, question their mutual consistency, and interpret the observed structures in terms of material parameters and boundary conditions.

References

Buiter, S.J.H, et al., The numerical sandbox: comparison of model results for a shortening and an extension experiment, The Geological Society of London Special Publication, 2006, 253, 29-64

Cubas, N., Barnes, C., Maillot, B. (2013), Inverse method applied to a sand wedge: estimation of friction parameters and uncertainty analysis, Journal of Structural Geology, 55, 101—113.

Cubas N., B. Maillot, C. Barnes, 2010. Statistical analysis of an experimental compressional sand wedge, Journal of Structural Geology, 32, 818–831, doi:10.1016/j.jsg.2010.05.010.

Cubas N., Y.M. Leroy, B. Maillot, Prediction of thrusting sequences in accretionary wedges, J. Geophys. Res., 113, B12412, doi:10.1029/2008JB005717, 2008.

Konstantinovskaya, E. & Malavieille, J. Erosion and exhumation in accretionary orogens : Experimental and geological approaches. Geochemistry, Geophysics, Geosystems, 2005, 6.

Maillot B., A sedimentation device to produce uniform sand packs, Tectonophysics, 593, 85—94, 2013, doi : 10.1016/j.tecto.2013.02.028.

Maillot B, Leroy YM. Kink-fold onset and development based on the maximum strength theorem. J. Mech. Phys. Solids. 2006, 54(10): 2030–2059.

Mary, B. C. L. Au delà du prisme critique de Coulomb par l'analyse limite séquentielle et contributions expérimentales, PhD thesis, Université de Cergy-Pontoise, France, 2012

Mary B.C., B. Maillot, Y.M. Leroy (2013), Predicting orogenic wedge styles as a function of analogue erosion law and material softening, Geochem. Geophys. Geosyst., 14, doi:10.1002/ggge.20262.

Mary BCL, Maillot B, Leroy YM. Deterministic chaos in frictional wedges revealed by convergence analysis. Int. J Num. Anal. Meth. Geom. 2013.

Pons A, Leroy YM. Stability of accretionary wedges based on the maximum strength theorem for fluid-saturated porous media . J. Mech. Phys. Solids . 2012, 60(4): 643–664.

Schreurs, G. et al., 2006: Analogue benchmarks of shortening and extension experiments, Buiter, S. & Schreurs, G. (Eds.) Geological Society Special publication, Analogue and Numerical Modelling of crustal scale processes., The Geological Society of London Special Publication, 2006, 253, 1-27

Souloumiac, P. Mécanismes 3D de ruine en géologie structurale : approche numérique et analogique. École Centrale Paris, 2009

Souloumiac P., B. Maillot, Y. M. Leroy, Bias due to side wall friction in sand box experiments, Journal of Structural Geology, 2012, doi:10.1016/j.jsg.2011.11.002.

Yuan, X., Y. M. Leroy, B. Maillot. Stability of over-pressured cohesive and frictional materials based on Sequential Limit Analysis, Extended Abstract, GeoMod 2014, this conference.

Cross-scale model of seismic cycle: first results

Iskander A. Muldashev[1], Stephan V. Sobolev[1]

[1] *GFZ German Research Centre for Geosciences, Potsdam, Germany*
e-mail: *muldashev@gfz-potsdam.de*
session: *(Seismo-) Tectonics*

Introduction

Origin and possible clustering of great earthquakes is perhaps one of the most exciting and mysterious problems in geophysics. Distribution in time of the largest earthquakes during observational period of about 100 years is highly uneven and shows two domains of increased release of seismic energy; during 50 s-60 s of last century and during the last decade, starting from great Sumatra earthquake of 2004. Interpretation of these data is highly controversial. Different statistical analyses suggest that such distribution indicates tendency for clustering of great earthquakes, or claim that this could be a realization of the random Poisson process, or that no robust statement on clustering can be made due to the small statistics for great earthquakes. Because it is unlikely that statistics of great earthquakes will significantly change in the next years, the uncertainty about clustering will remain. Therefore, other than purely statistical approaches should be found to tackle this problem.

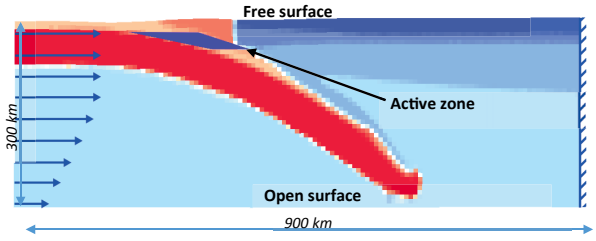

Fig. 1.: Setup of the 2D model of a subduction zone. Colours represent material phases. The region of the rate and state friction law is marked as active zone.

We take a modeling approach in which we attempt to model great earthquakes using numerical techniques that employ sophisticated rheology consistent with laboratory data of crustal and mantle rocks and are capable to describe geological time-scale deformation of lithosphere. Such geological time-scale models have been carried out for various tectonic settings using finite element modeling technique (Popov and Sobolev, 2008). Here we demonstrate first results of our modeling, which we consider as a preparation phase.

Modeling approach

First we make the model setup shown in Fig. 1, by modeling subduction process in the geological time-scale (107 years). We use finite element modeling technique (Popov and Sobolev, 2008) to model subduction during 4 Mln years, with the kinematic boundary conditions shown in Fig 1. To do so we employ visco-elasto-plastic rheology with constant low (0.01-0.05) friction coefficient in the uppermost part of the subduction slab, that is consistent with the idea of high pore-fluid pressure in subduction channel. The time step in such model is about 104 years. As a result we get the subduction model with appropriate stress distribution.

Second, we use geological time scale subduction model to simulate processes at the seismic cycle time scale (10-104 years). In these models we take geological time scale model, keep the same boundary conditions, but turn to much smaller time step (<10 years) and simultaneously introduce rate and state friction law (Dieterich, 1972;

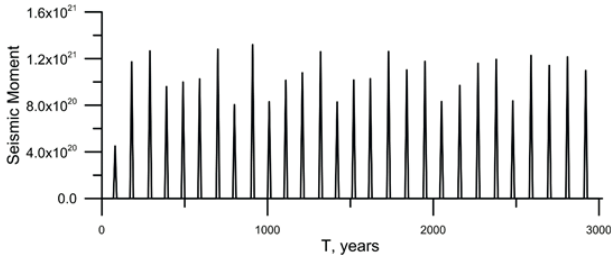

Fig. 2.: Seismic moment versus time for the typical model. Each "earthquake" represent one-time-step large displacement in "active zone" and in the adjacent deeper part of the interface between the slab and overriding plate.

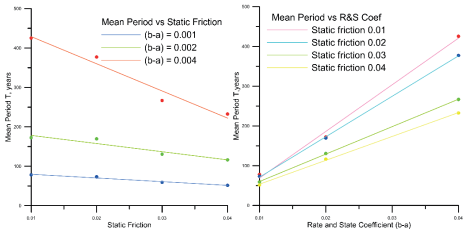

Fig. 3.: Mean period of earthquakes versus initial friction (left). Mean period of earthquakes versus rate and state coefficient (right).

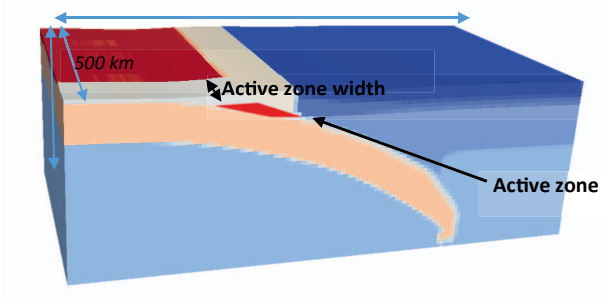

Fig. 4.: Setup of the 3D model of a subduction zone. Colours represent material phases. The region of the rate and state friction law is marked as active zone.

Scholtz, 1998) (in steady-state approximation) in the part of the uppermost layer of the subducting slab located in the depth range of (10 km to 42 km). This zone is labeled as "Active zone" in Fig. 1. The friction law is given by the relation:

$$\mu = \mu_0 - (b-a)log\Big(\frac{V}{V_0}\Big) \qquad (1)$$

Where μ_0 - static friction; a, b - experimentally determined variables; V - displacement rate; V_0 - initial displacement rate.

In the case when $(b-a) < 0$ the slip in "active zone" becomes unstable which leads to the stick-slip behavior (Scholtz, 1998), when instabilities (earthquakes) occur as one-time-step large displacements which are separated by period of slow inter-seismic deformation. Typical series of model earthquakes is shown in Fig. 2.

Parameter sensitivity

We performed a series of experiments to study sensitivity of models to different initial frictions and rate and state coefficients. Figure 3 shows dependencies of mean period between the earthquakes in model on static friction coefficient (Fig. 3, left) and on rate and state coefficient parameter (b-a) (Fig. 3, right).

As expected, we obtain almost linear relation between the earthquake period and (b-a) parameter. But interestingly, we also obtain week invers dependency of the earthquake period on static friction, that appears to be more pronounced at higher values of (b-a) parameter. We interpret this effect as the result of larger depth of brittle-ductile transition in the models with lower static friction that in turn causes deeper penetration of the rupture, larger average slip and larger time of accumulation of the next earthquake.

Next we study dependency of seismic moment (and average slip) of model earthquake on rupture area and compare the results with theoretical predictions. To do that we consider 3D model. Although we use 2D initial geological time-scale model, the active zone in the model is 3D (Fig. 4) with width varying from 100 km to 300 km. Rest of the model has static friction. In this setup static friction is 0.01 and (b-a) equals to 0.002. We use different sizes of finite elements in vertical cross-section (7 km) and in trench parallel direction (25 km to 50 km).

We obtain relations close to the theoretical expectation for the average stress drop of earthquake independent from its magnitude (Kanamori and Brodsky, 2004). For the smaller

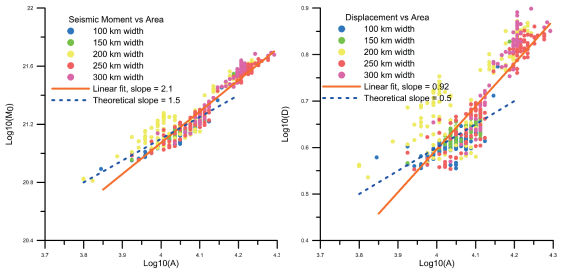

Fig. 5.: Logarithm of seismic moment of earthquakes versus logarithm of rupture area (left). .Logarithm of displacement during earthquake versus logarithm of rupture area (right).

earthquakes, whose rupture zones do not occupy the entire seismogenic zone, the average displacement is proportional to the square root of rapture area (A) and seismic moment is proportional to A3/2. For the large earthquakes the average displacement is proportional to the rapture area (A) and seismic moment is proportional to A2. These trends are also consistent with the observations (see Figure 11 in Kanamori and Brodsky (2004), suggesting that we are on the right way.

References

Dieterich, J. (1972), Time-dependence of rock friction. J. Geophys. Res. 77, 3690-3697.

Kanamori, H. and E.E. Brodsky (2004). The physics of earthquakes, Reports on Progress in Physics, v. 67, 1429-1496

A. A. Popov and S. V. Sobolev (2008), SLIM3D: A tool for three-dimensional thermomechanical modelling of lithospheric deformation with elasto-visco-plastic rheology. Physics of the Earth and Planetary Interiors 171, 55-75

Scholz, C. H. (1998), Earthquakes and friction laws, Nature, 391, 37-42.

Numerical modelling of the instantaneous subduction dynamics of the Banda Arc region

Casper Pranger[1,2], Cedric Thieulot[1], Arie van den Berg[1], Wim Spakman[1]

[1] *Mantle Dynamics Group, Department of Earth Sciences, Utrecht University, Budapestlaan 4, 3584 CD Utrecht, The Netherlands*
[2] *Now at Institute of Geophysics, ETH Zürich, Soneggstrasse 5, CH-8092 Zürich, Switzerland*
e-mail: *casper.pranger@erdw.ethz.ch*
session: *(Seismo-) Tectonics*

Introduction

The tightly curved Banda Arc (eastern Indonesia) plays a pivotal role in the convergent interaction of the Eurasian, Australian, and Pacific plates. Historically there have been two opposing hypotheses regarding its origin: either the arc has been formed by two opposite-dipping subduction zones joining at the apex, or a single slab has been wrought in its current position by surface kinematics and mantle processes. Using detailed tectonic reconstructions and mantle tomography, the latter view has recently gained substantial support by the work of Spakman and Hall (2010). Through numerical modelling of the instantaneous dynamics of the intricate subducting system, the research presented here aims to determine the factors that control the evolution of the single slab, but also to provide insight into the complexities of instantaneous numerical modelling of subduction in general. To aid the construction of very complex model geometries, we have developed a tool that allows us to digitally draw faults, slab sections, and plate outlines based on tomography, surface topography, and Wadati-Benioff zone geometry. The tool communicates with the finite element mesh generator, which then gives a composite mesh with highly desirable properties. Our results give a basic one-slab-model that satisfies both the predictions of the Spakman and Hall model and the stress state from CMT solutions and seismic fast directions. Better agreement can be attained by varying the buoyancy structure,

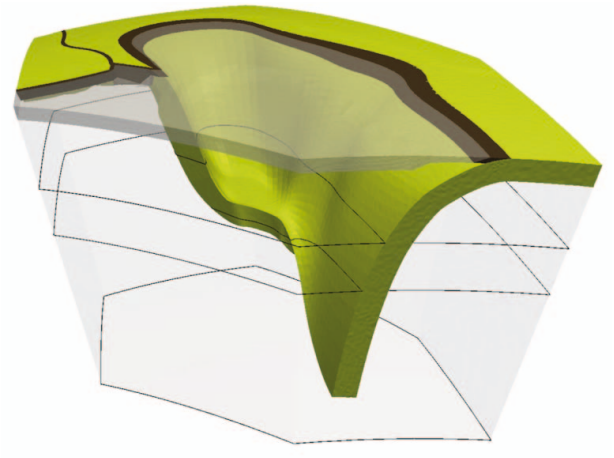

to which the behavior of the model is found to be rather sensitive. Additionally, we propose that a mantle flow component is required in order to maintain the northern slab limb in the case that it has detached from the surface lithosphere. In the absence of flow-induced resistance, our results suggests that further convergent motion can effect a transition towards large-scale slab detachment progressing southward if there is little buoyant support at the d660 phase transition.

References

Spakman, W., and R. Hall (2010), Surface deformation and slab–mantle interaction during banda arc subduction rollback, Nature Geoscience, 3 (8), 562–566.

Towards 3D seismo-thermo-mechanical models of the subduction thrust

Casper Pranger[1], Ylona van Dinther[1], Taras Gerya[1], Fabio Corbi[2,3], Francesca Funiciello[3]

[1] *Institute of Geophysics, ETH Zürich, Soneggstrasse 5, CH-8092 Zürich, Switzerland*
[2] *Earthquake and Volcano Physics, GFZ Potsdam, Telegrafenberg, 14473 Potsdam, Germany*
[3] *LET - Laboratory of Experimental Tectonics, Univ. "Roma Tre", L.S.L. Murialdo 1, 00146 Rome, Italy*
e-mail: *casper.pranger@erdw.ethz.ch*
session: *(Seismo-) Tectonics*

The recent development of numerical seismo-thermo-mechanical (STM) models bridges the gap between geodynamic and seismic timescales and thereby links long-term deformation and subduction dynamics to short-term seismogenesis (e. g., van Dinther et al., 2013, 2014). Complementing dynamic rupture models of a priori defined fault planes, this approach allows for spontaneous emergence of rupture paths, both on and off the megathrust, through slow tectonic loading, rate-dependent friction, and visco-elastic relaxation.

In twin papers (Corbi et al., 2013; Van Dinther et al., 2013), the STM technique has been robustly validated with laboratory models of a deforming visco-elastic gelatine wedge (Figure 1 a). In these laboratory models, the gelatine wedge is fixed at the backstop while being dragged in the down-dip direction at the base. A seismogenic zone is formed on this base by locally introducing a gelatine-sandpaper interface with strainrate-weakening characteristics, which is superseded in the up-dip and down-dip limits by a gelatine-plastic strainrate-strengthening interface. In a 2D center-line vertical section of the gelatine wedge, particles are observed moving away from the trench during co-seismic time intervals (cf. Figure 2 a), while during the seismic event they surge towards the trench (cf. Figure 2 b).

While the center-line sampling of the semi-2D laboratory setup (constant along-strike) should

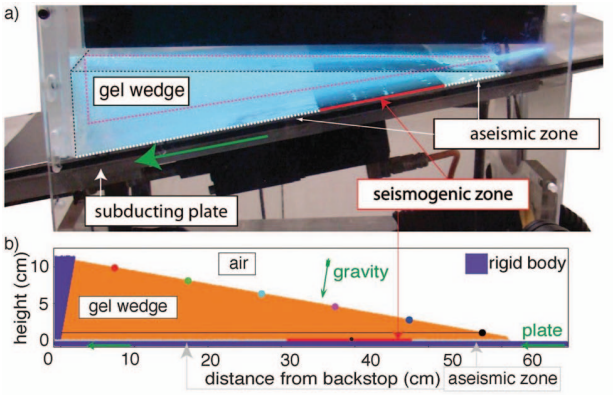

Fig. 1.: a) Laboratory setup. A visco-elastic gel wedge is dragged in the down-dip direction by a subducting plate, but is prevented from transportation by the backstop (left). b) Numerical replica of the laboratory setup, slightly rotated to allow for easier implementation. Note that the body force component is rotated accordingly.

inhibit the detrimental effects of the strike-normal boundaries, it is now clear from top-view surface particle motion measurements that 3D phenomena are substantial (Corbi and Funiciello, pers. comm.): many seismic events nucleate close to the lateral side-walls and pass through the center-line section only transiently, which may lead to an underestimation of slip area, slip magnitude, and seismic moment magnitude.

While the center-line sampling of the semi-2D laboratory setup (constant along-strike) should inhibit the detrimental effects of the strike-normal

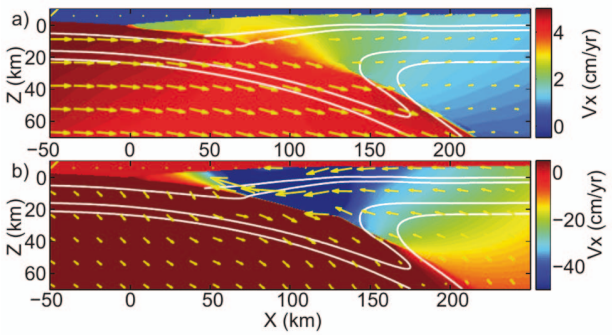

Fig. 2.: a) Locking, and b) seismic release in a numerical STM model of self-consistent subduction (van Dinther et al., 2014).

boundaries, it is now clear from top-view surface particle motion measurements that 3D phenomena are substantial (Corbi and Funiciello, pers. comm.): many seismic events nucleate close to the lateral side-walls and pass through the centerline section only transiently, which may lead to an underestimation of slip area, slip magnitude, and seismic moment magnitude.

By incorporating the existing STM functionality and elasticity into the 3-dimensional finite difference code I3ELVIS (Zhu et al., 2009), we will be able to perform a more exhaustive validation test against results obtained in the laboratory. In the future, a new generation of 3D STM models will allow us to investigate the full spatio-temporal source parameter distribution of on- and off-megathrust events in (real-Earth) subduction zones.

References

Corbi, F., F. Funiciello, M. Moroni, Y. van Dinther, P. M. Mai, L. A. Dalguer, and C. Faccenna (2013), The seismic cycle at subduction thrusts: 1. Insights from laboratory models, J. Geophys. Res. Solid Earth, 118, 1483-1501, doi:10.1029/2012JB009481.

van Dinther, Y., T. V. Gerya, L. A. Dalguer, F. Corbi, F. Funiciello, and P. M. Mai (2013), The seismic cycle at subduction thrusts: 2. Dynamic implications of geodynamic simulations validated with laboratory models, J. Geophys. Res. Solid Earth, 118, 1502-1525, doi:10.1029/2012JB009479

van Dinther, Y., T. V. Gerya, L. A. Dalguer, P. M. Mai, G. Morra, and D. Giardini (2014), The seismic cycle at subduction thrusts: insights from seismo-thermo-mechanical models, J. Geophys. Res.: Solid Earth, doi:10.1029/2013JB010380.

Zhu, G., T. V. Gerya, D. A. Yuen, S. Honda, T. Yoshida, and J. A. Connolly (2009). Three-dimensional dynamics of hydrous thermal-chemical plumes in oceanic subduction zones. Geochemistry, Geophysics, Geosystems, 10(11).

Smart or Beautiful? Accretionary wedge evolution seen as a competition between minimum work and critical taper

Tasca Santimano[1], Matthias Rosenau[1], Onno Oncken[1]

[1] *Deutsches GeoForschungsZentrum GFZ Potsdam, Germany*
e-mail: *tsanti@gfz-potsdam.de*
session: *(Seismo-) Tectonics*

Introduction

Accretionary wedge evolution has been described by two theories: The Critical taper theory (CTT, Davis et. al., 1983) and the minimum work concept (MWC, Masek & Duncan, 1998). CTT is based on force balance and predicts the ideal ("beautiful") shape (critical taper, CT) of an accretionary wedge system and its tectonic regime (extensive, compressive, stable). However, it does not specify which structures are formed and reactivated to reach the preferred geometry during accretionary wedge growth. The latter can be predicted by MWC which states that deformation is accommodated in a energetically "smart" way by faults that allow to minimize total (frictional plus gravitational) work. In this study we test the applicability and interplay of both concepts to accretionary wedge growth by analysing the evolution of a homogeneous sand wedge. We describe geometry changes and the work done through accretion cycles and hypothesize that there is a competition between minimizing work and reaching the critical taper that controls the evolution of accretionary wedges.

Experimental setup and analysis methods

The experimental setup consists of a sandbox that creates a typical plane strain compressional sand (friction coefficient ~ 0.7) wedge with a low friction basal detachment (glass beads, friction coefficient ~ 0.45) by pulling the sand layer against a rigid backwall. The evolution of the wedge is recorded from the side using CCD (charge coupled device) cameras whose sequential images are analysed by means of the Particle Image Velocimetry (PIV). This allows for a time-series collection of the incremental geometries and internal displacement fields (velocity) of the entire wedge. The topographic peak (crest) and the tip of the wedge were assigned active wedge height and length (H, L), are used for calculating the wedge slope ($\arctan(\frac{H}{L})$). The vertical component (D_y) of the resulting vector field (i. e. uplift against gravity g) and the horizontal component (D_x, basal displacement against basal friction μ) are used to calculate the gravitational (W_g) and frictional (W_f) work done by the wedge with weight W, respectively ($W_g = WD_y$ and $W_f = WD_x\mu$). Observed geometrical evolution and work history has finally been compared to analytical solutions of a self-similarly growing and critically tapered wedge.

Observations and analytical results

Accretion cyclicity

The wedge evolves in a typical cyclic manner of accretion resulting in saw-tooth like growth curves in height, length and slope (Fig. 1 A, 1 B). An accretionary cycle involves the localization of strain to form a new set of conjugated thrust and back thrust. While the backthrust is quickly abandoned, displacement along the forethrust continues until the end of the accretionary cycle

when a new fault is formed. The wedge allows for both frontal accretion and sporadic deep underthrusting and basal accretion due to smearing of the ramp and shallow detachment by entrained glass beads. Long underthrust episodes are always followed by a short frontal accretion cycles resulting in a bimodal periodicity of accretion.

Geometric evolution

After a short initiation phase the wedge develops towards a stable wedge taper ($\sim 10°$) with systematic fluctuations associated with accretionary cycles (Fig. 1 A). Wedge length and height grow according to a power law again with fluctuations associated with accretionary cycles (Fig. 1 B). Longterm trends fit well to the analytical predictions of self-similar wedge growth. Importantly geometrical predictions are met at the onset of an accretionary cycle. During accretion, wedge geometry evolves away from the predictions by shortening and uplift towards higher slopes, i. e. into the stable (or locally even extensional) CT regime.

Work done

Work analysis shows (Fig. 1 C) that gravitational work is significantly lower than frictional work. This is because vertical displacement is generally less than horizontal displacement of the wedge. On a long time scale, frictional work increases as the wedge grows and the basal detachment area increases, however gravitational work reaches an upper bound because uplift ceases naturally as the wedge grows. Total work increases consistently as the wedge grows. Longterm trends fit at first order scale to the analytical predictions of a self-similar wedge growth. Looking at shorter timescales, total work is minimized and closest to the theoretical predictions at the end of the accretion cycle. At the onset of a new accretion cycle, gravitational work is minimized but increases subsequently as the active thrust ramp penetrates deeper into the wedge (i. e. uplifts successively larger volumes). Frictional work, in contrast, is maximized at the onset of a new accretion cycle and subsequently minimized because the length of the shallow flat increases at the cost of the deep flat of the thrust as the active thrust ramp penetrates into the wedge.

Discussion, Conclusions & Implications

The analysis above shows that sand wedges might be both smart and beautiful but not at the same time: The preferred CT geometry is met only at the beginning of a new accretion cycle while work is minimized at the end of an accretionary cycle. Compared to a self-similarly growing wedge which can be viewed as an ideal, always smart and always beautiful wedge growing by infinitesimal basal accretion of diffuse deformation, real accretionary wedges obviously switch between states consistent with CTT and MWC. Underthrusting appears to be the energetically preferred path of accreting material but leads to shortening and uplift of the wedge. Shortening and uplift steepens the wedge and therefore causes its departure from the critical state. The latter can only be re-established by forming a new, energetically unfavorable frontal thrust ahead of the wedge tip lowering the taper.

Fig. 1 D is a synoptic plot of the geometric and energetic performance of the wedge. The ideal (smart and beautiful) state is at the origin of this plot where predicted and observed slope and work are the same. Obviously, accretionary cycles cannot reach the ideal state easily but rather circles between energetically vs. geometrically optimized states at progressively decreasing distance from the origin. When comparing observed values to the predicted values of work and slope done by the wedge respectively, the deviation of the observed values from the predicted value becomes minimized immediately before and after thrust formation, respectively. It follows that accretionary wedges are described in rare instances (around the formation of a new thrust) by either CTT or MWC. Instead, most wedge stages reflect the competition of reaching criticality and minimum work, i. e. are a mixture between a geo-

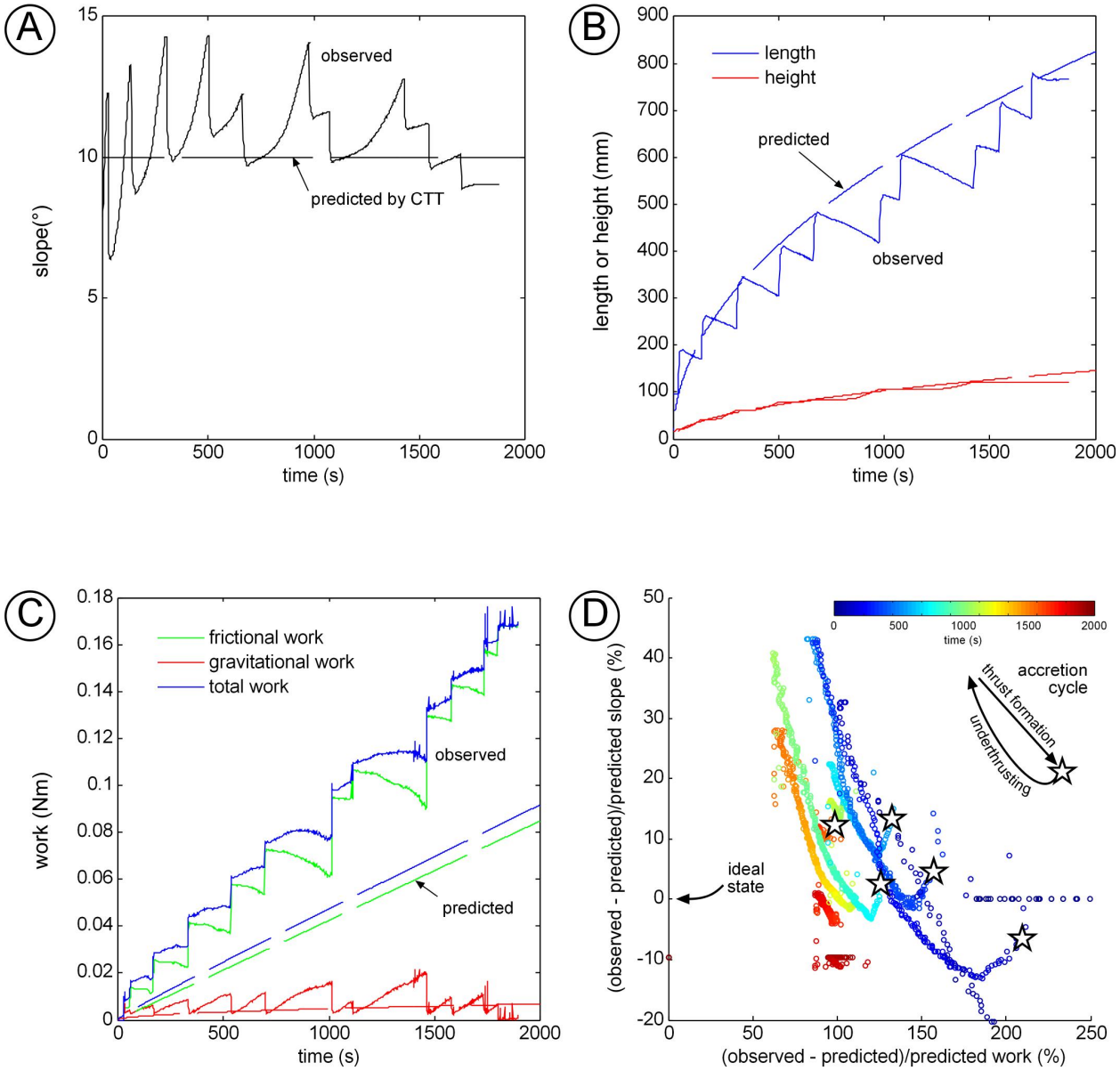

Fig. 1.: Geometrical wedge evolution and work done: (A) slope vs. time, (B) height and length vs. time, (C) work vs. time. Analytical solutions from self-similar wedge growth indicated by stippled trends, (D) Synoptic plot of wedge performance: Normalized deviation of observed slope values from the predicted slope values (%) vs. normalized deviation of observed work values from the predicted work values (%).

metrically versus an energetically preferred state. The analysis implies that inferences on wedge mechanics from natural observations based on CTT and MWC should be drawn only during the formation of a new frontal thrust. Only very mature wedges composed of several tens of accreation cycles might be able to reach a state where both geometry and work are optimized through the accretionary cycle (i. e. the origin in Fig. 1 D).

References

Davis, D., Suppe, J., Dahlen, F.A., 1983: Mechanics of Fold-and-Thrust Belts and Accretionary Wedges. Journal of Geophysical Research 88, 1153-1172.

Masek, J.G., Duncan, C.C., 1998: Minimum-work mountain building. Journal of Geophysical Research, 103,907-917.

CHANDRAYAAN-1 data infers tectonic activity on the south pole of the moon

Priyadarshini Singh, Saumitra Mukherjee

School of Environmental Sciences, Jawaharlal Nehru University, New Delhi – India
e-mail: *ps.sesjnu@gmail.com*
session: *(Seismo-) Tectonics*

Introduction

Morphological characteristics of the moon were studied using data strips from the miniature synthetic aperture radar (Mini-SAR) payload onboard CHANDRAYAAN-1 mission. Fault lines and rocky avalanches developed post dislocation along such fault zones within the South Polar Region have been identified in this study. Also, the identified features show morphological similarity to the features seen on terrestrial surfaces. Mini-SAR imaging radar onboard CHANDRAYAAN-1 mission was the first mono-static lunar orbiting synthetic aperture radar (SAR). It conveniently reveals various crater features in completely or partially shadowed regions of the lunar poles on the surface as well as the lunar regolith [Mohan et al., 2011; Spudis et al., 2009]. Previous studies investigating lunar tectonic activity have used optical data primarily to study lunar tectonics. However, active remote sensing using microwave data has helped in studying the lunar topography in order to demarcate unique features otherwise not visible from simple optical data due to the ability of microwaves to reveal images of shadowed regions as well as penetrating the surface regolith [Mohan et al., 2011]. Optical images from Wide Angle Camera onboard the Lunar Reconnaissance Orbiter Camera (LROC) have also been used alongside the SAR data to pinpoint regions falling within shadowed parts of the lunar south pole. It is being reported that the lunar surface morphology is largely governed by these tectonic perturbations. Further it has been found out that cosmic rays and solar wind flux variability coupled with the interior tectonic activity and meteorite impact has given the tectonic activity of the moon. This finding is supported by the manifestation of tectonic activities on the moon in the form of faults and related dislocations. Present work confirms that partially and completely shadowed crater interiors present in the Polar Regions contain unique features indicative of tectonic activity. The study therefore focuses on the identification of these features indicating the presence of faults/lineaments/fractures on the lunar topography.

Study area and methodology

The study area falls within the south polar region of the moon lying within Cabeus B crater. Cabeus B is an impact crater centered at 82°18′ S and 54°12′ W with a diameter of ~61 km. Stokes parameters (S_0, S_1, S_2 and S_3) and degree of polarization (m) were derived for each pixel using ENVI software to generate $m - \chi$ decomposition images (Raney et al., 2007). Stokes Parameters (S_0, S_1, S_2 and S_3), degree of polarization (m) and $m - \chi$ scattering contributions were calculated for each pixel on ENVI software using the following band math equations. Each pixel in an image strip consisted of 16 bytes data in four channels of 4 bytes each as $|\mathrm{LH}|_2$, $|\mathrm{LV}|_2$, Real $(\mathrm{LH} \cdot \mathrm{LV}^*)$ and Imaginary $(\mathrm{LH} \cdot \mathrm{LV}^*)$ [Mohan et

al., 2011].

$$S = \begin{bmatrix} S_0 &=& \langle |E_{\mathrm{LH}}|^2 + |E_{\mathrm{LV}}|^2 \rangle \\ S_1 &=& \langle |E_{\mathrm{LH}}|^2 - |E_{\mathrm{LV}}|^2 \rangle \\ S_2 &=& 2\Re e \langle E_{\mathrm{LH}} E_{\mathrm{LV}}^* \rangle \\ S_3 &=& -2\Im m \langle E_{\mathrm{LH}} E_{\mathrm{LV}}^* \rangle \end{bmatrix} \quad (1)$$

where E_{LH} and E_{LV} are the electric fields for the horizontal and vertical linear polarizations received respectively, and the averages are time or spatial averages and * represents the conjugate of the complex number.

Reference [3] equations were used to calculate the degree of polarization (m). Reference [4] and [5] were used to calculate the degree of circularity (χ) and $m - \chi$ scattering contributions for each pixel on ENVI software. The equations used are as follows:

$$m = \frac{\sqrt{S_1^2 + S_2^2 + S_3^2}}{S_0} \quad (2)$$

$$B = \sqrt{\frac{S_0 m \left(1 - \sin\left(2\chi\right)\right)}{2}} \quad (3)$$

$$G = \sqrt{S_0 \left(1 - m\right)} \quad (4)$$

$$R = \sqrt{\frac{S_0 m \left(1 + \sin\left(2\chi\right)\right)}{2}} \quad (5)$$

Here blue (B) indicates single-bounce (Bragg) backscattering, green (G) represents the randomly polarized constituent or volume scattering and red (R) corresponds to double-bounce scattering.

Results and Discussion

Cabeus B is a relatively large impact crater having several small impact craters on its floor. After applying $m - \chi$ decomposition technique to the mini-SAR data, a distinct fault line was observed traversing the floor of the northern wall of the crater and reaching till the southern end before it disappears beneath a debris avalanche lying on the southeastern wall. Both the debris avalanche and the fault line are not visible on optical wide angle camera image. Alternately, these features can be distinctly seen on the $m - \chi$ decomposition image. The neighboring areas lying beyond the rim of Cabeus B also have extensions of the inferred fault lines traversing regions lying within and extending up to neighboring craters around Cabeus B.

The debris avalanche lying at the visible southern end of the identified fault line can be seen on the optical image as a faint structure. On $m - \chi$ decomposition image, however, this feature can be seen distinctly covered with green pixels due to volume scattering. It extends from the tip of the south eastern inner wall of the crater and end at the floor of the crater. The fault line disappears beneath this debris avalanche. There is a possibility that the formation of the debris avalanche has taken place due to dislocation and seismic shaking along the identified fault line.

References

[1] S. Mohan, A. Das and M. Chakraborty, "Studies of polarimetric properties of lunar surface using Mini-SAR data," Current Science, vol. 101, no. 2, pp. 159-164, 2011.

[2] P. Spudis, S. Nozette, B. Bussey, K. Raney, H. Winters, C.L. Lichtenberg, W. Marinelli, J.C. Crusan and M.M. Gates, "MiniSAR: an imaging radar experiment for Chandrayaan-1 mission to the Moon", Current Science, vol. 96, no. 4, pp. 533-539, February 2009.

[3] R.K. Raney, "Hybrid-polarity SAR architecture", IEEE Trans. Geosci and. Remote Sensing, vol. 45, no. 11, pp. 3397-3404, November 2007.

[4] R.K. Raney, J.T.S. Cahill, G.W. Patterson, and D.B.J. Bussey, "The m-chi decomposition of hybrid dual-polarimetric radar data", IEEE International IGARSS, pp. 5093-5096, 2012.

[5] R. K. Raney, J.T.S. Cahill, G. W. Patterson, D. Benjamin, J. Bussey and the Mini-RF Team, "Characterization of lunar craters using m–χ decompositions of mini-RF radar data", LPSC, Abstract no. 2380, 2012.

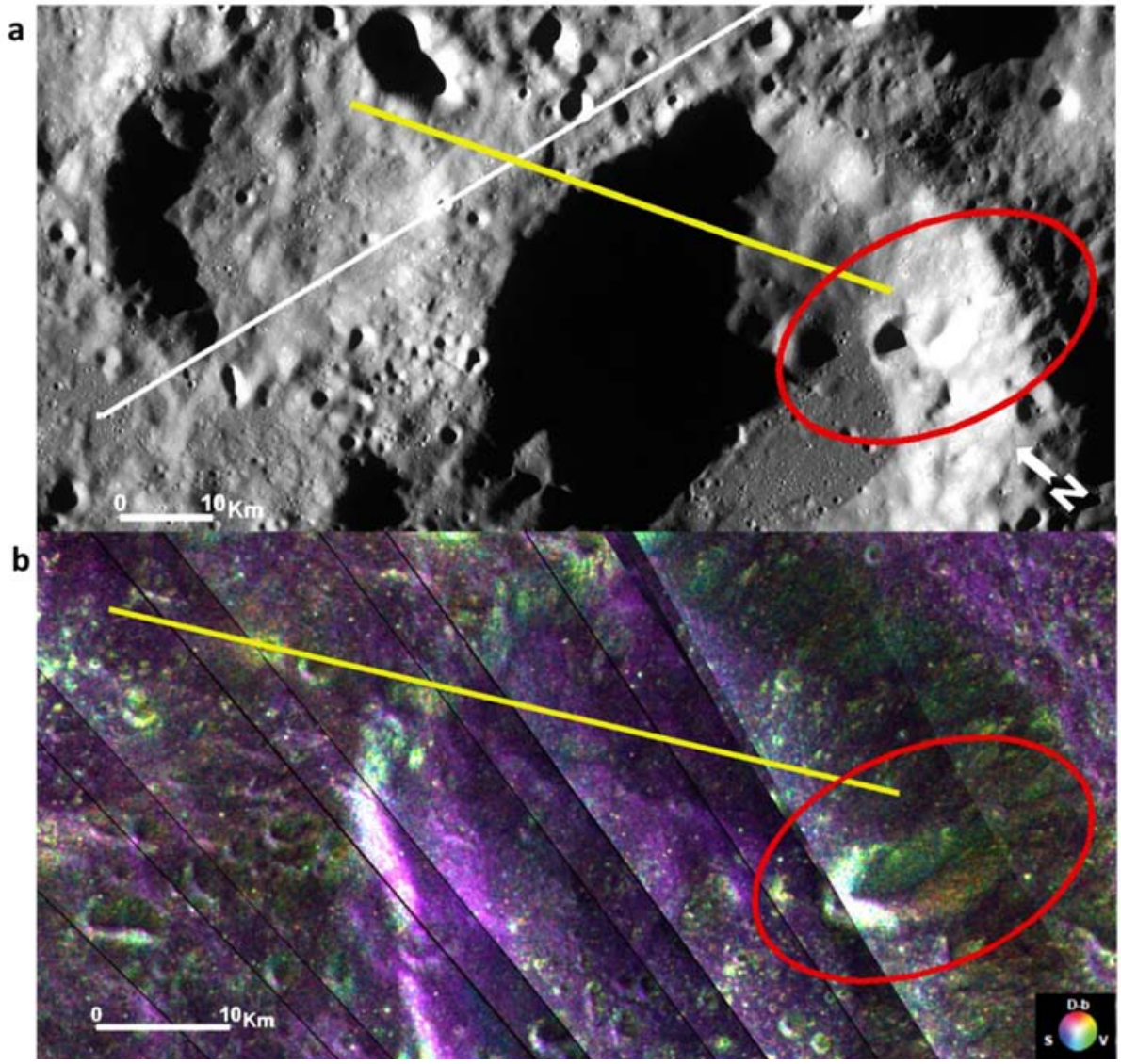

Fig. 1.: Fault lines and debris avalanche within Cabeus B (centered at $82°18'$ S and $54°12'$ W). **a.)** Wide Angle Camera image of Cabeus B crater and surrounding region with the inferred fault lines and the debris avalanche marked with red ellipse. **b.)** $m - \chi$ decomposition image of the region in a.); fault line invisible in optical image can be seen lying below the length of the yellow line; the debris avalanche marked with red ellipse visible clearly with green pixels from volume scattering showing the rough surface due to the debris.

The concepts of complex network advance understanding of earthquake science

Norikazu Suzuki

College of Science and Technology, Nihon University, Chiba, 274-8501, Japan
e-mail: *suzu@phys.ge.cst.nihon-u.ac.jp*
session: *(Seismo-) Tectonics*

Seismicity is governed by yet unknown dynamics of the earth crust as a complex system. Although seismology has a long tradition, only a few universal laws have been discovered. The celebrated examples are the Omori law (Omori 1894) for the temporal pattern of aftershocks and the Gutenberg-Richter law (Gutenberg and Richter 1949) for the scaling relation between frequency and magnitude. Although there are some discussions about the theoretical bases of these laws, it seems fair to say that essentially they still remain empirical. The situation shows how understanding physics of earthquakes is far from maturity. And, there may be much to be explored even at the empirical level. This in turn suggests a possibility that approach from the viewpoint of science of complexity may shed new light on seismicity.

In the recent investigations (Abe and Suzuki 2003, 2005a), we have analyzed the spatio-temporal properties of seismicity from the viewpoint of nonextensive statistical mechanics. Nonextensive statistical mechanics is constructed based on the Tsallis entropy (Tsallis 1988) and generalizes Boltzmann-Gibbs statistical mechanics in order to treat complex systems. We have found that both the spatial distance and time interval between two successive earthquakes are well described by the q-exponential distributions, which are characteristics of nonextensive statistical mechanics and maximize the Tsallis entropy under appropriate constraints. The fact that two successive earthquakes obey such definite statistical laws implies that successive events are indivisibly correlated, no matter how large their spatial distance is. In fact, there is a report (Steeples and Steeples 1996), which shows that an earthquake can be induced by a foregoing earthquake more than 1000 km away. Furthermore, it is known that, after the big earthquake M=9.0 in Japan three years ago, the seismic wave traveled the whole surface of the earth at least 5 times. This seismic wave actually triggered many subsequent earthquakes in Japan, China, Canada, Mexico and U.S.A. (Peng et al. 2013). This means that the seismic correlation length may be enormously large, indicating a strong similarity to phase transition phenomena and making it inappropriate to put spatial windows in analysis of seismicity, in general. Thus, we are naturally led to a conclusion that the earth crust always stays in a critical state.

Now, in contemporary science, the concept of complex networks is receiving much attention. The research in this direction was initiated by the works of Watts and Strogatz (1998) on small-world networks and of Barabási and Albert, (1999) on scale-free networks. A main purpose of this research area is to understand the topological and dynamical properties appearing in the network structure behind various complex systems, such as collaboration of actors, citation pattern of scientific papers, metabolic networks, social networks, WorldWideWeb, electrical power grids, and so on. Common features among these are that they are scale-free networks with power-law connectivity distributions and are small-world ones characterized by large values of the cluster-

ing coefficient as well as small values of the characteristic path length. In particular, the model proposed by Barabási and Albert (1999), which assumes network growth combined with the so-called preferential attachment rule, is known to generate scale-free networks.

As mentioned above, two successive events obey the definite statistical laws. It indicates that successive events are indivisibly correlated each other. This motivates us to describe seismicity by making use of a network, in which vertices and edges represent events and their correlations, respectively. In this way, novel aspects of seismicity as a complex phenomenon are expected to be revealed.

In this talk, we discuss a novel method of describing complexity of seismicity, which has recently been introduced in the literature (Abe and Suzuki 2004 a, 2006 a). The seismic data are mapped to growing random networks. Vertices and edges of such networks correspond to coarse-grained events and event-event correlations, respectively. Yet unknown microscopic dynamics governing event-event correlations and fault-fault interactions is replaced by these edges. Global physical properties of seismicity can then be explored by examining its geometric (e. g., topological etc.), statistical and dynamical properties.

Firstly, we show that the earthquake network is scale free (Abe and Suzuki 2004 a, 2006 a), being characterized by the power-law connectivity distribution (Figure 1) . We give a physical interpretation to this result based on network growth with the preferential attachment rule (Barabási and Albert 1999) together with the Gutenberg-Richter law (Gutenberg and Richter 1949).

Secondly, we study the small-world structure of the earthquake network reduced to an undirected simple network (Abe and Suzuki 2004 b, 2006 a). The value of the clustering coefficient is found to be much larger than that of the classical random network. In addition, the average path length is very small.

Thirdly, we show that the earthquake network possesses hierarchical organization (Abe and Suzuki 2006 b). We interpret this fact in terms of vertex fittness and vertex deactivation by the process of stress release at faults.

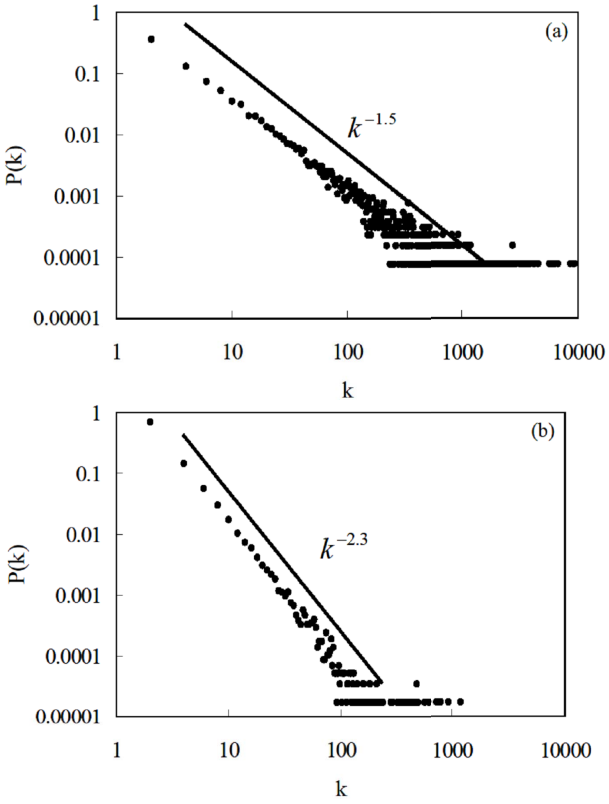

Fig. 1.: The log-log plots of the connectivity distributions of the earthquake networks P(k) in (a) California and (b) Japan.

Fourthly, we find that the earthquake network has the property of assortative mixing (Abe and Suzuki 2006 b). This point is an essential difference of the earthquake network from the Internet that has disassortative mixing.

Finally, we report the discovery of a scale-invariant law of the period distribution in the directed earthquake network (Abe and Suzuki 2005 b), which indicates that after how many earthquakes an earthquake returns to the initial location. This result manifests a fundamental difficulty in statistically estimating the value of period.

Combined with other dynamical properties (Suzuki 2012, Abe and Suzuki 2007, 2009 a, 2009 b, 2009 c, 2012 a, 2012 b), the present results imply that yet unknown mechanism governing seismicity may be so-called glassy dynamics (Abe and Suzuki 2004 c, 2012 c) on a growing complex

network. These observations have obvious importance for constructing and improving physical models of seismicity such as the ones exhibiting self-organized criticality.

References

Abe, S., Suzuki, N. (2003).: Law for the distance between successive earthquakes. J. Geophys. Res. 108, B2, 2113-2117.

Abe, S., Suzuki, N. (2004a): Scale-free network of earthquake. Europhys. Lett., 65, 581-586.

Abe, S., Suzuki, N. (2004b): Small-world structure of earthquake network. Physica A 337, 357-362.

Abe, S., Suzuki, N. (2004c): Aging and scaling of earthquake aftershocks. Physica A 332, 533-538.

Abe, S., Suzuki, N. (2005a): Scale-free statistics of time interval between successive earthquakes. Physica A 350, 588-596.

Abe, S., Suzuki, N. (2005b): Scale-invariant statistics of period in directed earthquake network. Eur. Phys. J. B, 44, 115-117.

Abe, S., Suzuki, N. (2006a): Complex-network description of seismicity. Nonlin. Processes Geophys., 13, 145-150.

Abe, S., Suzuki, N. (2006b): Complex earthquake networks: Hierarchical organization and assortative mixing. Phys. Rev. E, 74, 026113 p1-p5.

Abe, S., Suzuki, N. (2007): Dynamical evolution of clustering in complex network of earthquake. Eur. Phys. J. B, 59, 93-97.

Abe, S., Suzuki, N. (2009a): Earthquake networks, complex. in Encyclopedia of Complexity and Systems Science, Springer, New York, 2530-2538.

Abe, S., Suzuki, N. (2009b): Determination of the scale of coarse graining in earthquake networks. EPL, 87, 48008 p1-p5.

Abe, S., Suzuki, N. (2009c): Violation of the scaling relation and non-markovian nature of earthquake aftershocks. Physica A, 388, 1917-1920.

Abe, S., Suzuki, N. (2012a): Universal law for waiting internal time in seismicity and its implication to earthquake network. EPL, 97, 49002 p1-p5.

Abe, S., Suzuki, N. (2012b): Dynamical evolution of the community structure of complex earthquake network. EPL, 99, 39001-p1-p4.

Abe, S., Suzuki, N. (2012c): Aftershocks in modern perspectives: Complex earthquake network, aging, and non-Markovianity, Acta Geophysica, 60, 547-561.

Barabási, A-L., Albert, R. (1999): Emergence of scaling in random networks, Science. 286, 509-512.

Gutenberg, B., Richter, C.F. (1949): Seismicity of the earth and associated phenomena. Princeton University Press, Princeton.

Omori, F. (1894), On the aftershocks of earthquakes, J. Coll. Sci. Imp. Univ. Tokyo, 7, 111– 216.

Peng, F., Gonzalez-Huizar, H., Chao, K., Aiken, C., Moreno, B., Armstrong, G. (2013): Tectonic Tremor beneath Cuba Triggered by the Mw 8.8 Maule and Mw 9.0 Tohoku-Oki Earthquakes, Bull. Seismol. Soc.Am. 103 595-600.

Steeples, D.W., and Steeples, D.D. (1996): Far-field aftershocks of the 1906 earthquake, Bull. Seismol. Soc. Am. 86, 4, 921-924.

Suzuki, N. (2012): Complex network of earthquakes: Universal law for waiting internal time in seismicity. in Proceedings of 8th International Conference on Signal Image Technology and Internet Based systems (IEEE Computer Society), 707-709.

Tsallis, C. (1988), Possible generalization of Boltzmann-Gibbs statistics, J. Stat. Phys., 52, 479– 487.

Watts, D. J., Strogatz, S. H. (1998): Collective dynamics of 'small-world' networks. Nature, 393, 440-442.

Hypothesis of geodynamic processes in the lithosphere under catastrophic earthquake Tohoku-Oki

V. N. Tatarinov, A. I. Kagan, T. A. Tatarinova

Geophysical Center of Russian Academy of Sciences, 117296, Moscow, Molodezhnaya 3
e-mail: *victat@wdcb.ru*
session: *(Seismo-) Tectonics*

Earthquake Tohoku-Oki, 11.03.2011 happened near the island of Honshu, has attracted attention not only for its energy capacity and catastrophic consequences of tsunami and the destruction of three nuclear reactors, "Fukushima-1", but also a unique experimental data on the co-seismic and post-seismic vertical and horizontal displacements of the Earth's crust in the area of the Japanese archipelago, which were received on geodynamic network GEONET (GNSS Earth Observation Network System).

The new facts gave rise to the construction of various geodynamic models of the region [1-3]. Almost all of them are based on postulates plate-tectonics under which earthquakes occurring in this region is the result of military pressure on the Eurasian continental plate (EP), the subducting Pacific plate under it (PP).

In inherently discussion tectonic "fixists" and "mobilists" victory on the side of the second, because still supported by a majority of geodynamic models of seismicity of the region, based on the primacy of force action PP. However, there are a number of fundamental contradictions that do not explain or do not notice.

In this connection, based on the analysis and synthesis of evidence on the kinematics of the upper lithosphere during and after the earthquake Tohoku-Oki as the subject for discussion Alternative hypotheses about the sources of power such catastrophic earthquakes occurring in the area of Japanese islands.

GPS-observations confirmed facts displacement of the upper part of the lithosphere caused by earthquakes in the eastern direction during earthquakes with magnitude M $>$ 7.5 [4-6] , suggest that over the past 100-120 years, the Japanese archipelago has shifted in the direction of the oceanic plate at a distance 10 m to 14 m. If we take the maximum speed of horizontal movements PP westboundfor 100 – 120 years it should integrally displaced approximately 10 m. Thus, the horizontal displacement of the oceanic plate in a westerly direction and reverse "rollback" edge of the Eurasian plate to the east by earthquakes in the mentioned period are comparable with each other.

Analysis of the available experimental data on seismicity, structure and deformation of the lithosphere, and the results of modeling and reconstruction stress on parameters of the earthquake led to the following conclusions.

1. Seismicity:
    - Japan Earthquake type occur at depths of up to 700 km, while the deeper the earthquake, the more the area in which it is felt;
    - Post-seismic motion capture vast territory, so at Tohoku-Oki earthquake displacement were recorded on a third of the Amur plate, the transverse dimensions of up to 1000 km, indicating that the deep nature of the source;
    - Development of the earthquake stepwise character and a huge area (not linear fracture) total rupture plane – about 200 km to 400 km. The type of

motion in the outbreak of catastrophic earthquakes - thrust with thrust;

- Location of earthquake foci almost to the border of the asthenosphere (700 km) in the marginal part of the continental plate, allows you to "seditious" assumption about the prevalence in the area to the specified depth of the horizontal components of stress. And just below this limit, the rocks are in hydrostatic stress state. At the edge of the oceanic plate boundary transition in hydrostatic condition is probably much higher and is determined Moho discontinuity, about 10 km. This assumption of asymmetric stress state plots pairing the continental and oceanic plates form the basis of the hypothesis of the power source of catastrophic earthquakes in the area.

2. Features of the structure of the lithosphere
   - According to the seismic tomography across the Pacific border land registered relatively more resilient species (up to 5 %), the incident angle of $50° - 60°$, the power of which is 5 – 7 times greater than the thickness of the oceanic crust. In the upper mantle of the North American plate in the core is firmer deeper part (depth interval - 200 km to 600 km), and the inactive part of the board - only the upper part to a depth of 400 km. In tectonically active zone of continental plates at a depth of an extensive area of intense (elastic) rocks. As suggesting she may be considered as a potential energy source that initiates the destruction of the environment on the outskirts of the lithosphere plates.

3. Postseismic horizontal and vertical movement
   - Nature of post-seismic motions according to the following GPS-observations. Vertical movement: the eastern part falls, rises west (maximum positive movement in the area of focus to 3 m). Horizontal movement: directed toward the hearth (maximum displacements up to 24 m);
   - There is an approximate equality of the absolute values of the displacement of the Pacific plate and the "reverse recoil" at the edge of the Eurasian plate earthquakes over the past 100 a to 200 a;
   - No significant positive vertical movements edge of the Eurasian plate in the face of pressure on her Pacific plate in between earthquakes.

4. Reconstruction of stress on the earthquake source
   - Oceanic trench is a boundary separating two domains of the geodynamic regime: horizontal compression (to the west of the trough) and stretching (east);
   - The orientation of the principal compressive stress varies from west to east from $45°$ to $0°$ and $-90°$ for the deep-sea trench [7]. Thus for gutter earthquake situation corresponds horizontal extension.

A hypothesis on the origin of power sources geodynamic Japan earthquake type which, without explaining the reasons for internal model (as is usually done), repelled from the actual material (Fig.1).

1. Elastic energy accumulation occurs in the deep parts of the continental plates where the maximum stresses exist, as rocks retain their elastic properties. This depth can be evaluated by the maximum depth of earthquakes - 700-600 km. Indirectly, this confirms the earthquake that occurred May 24, 2013 in the Okhotsk Sea at a depth of 600 km of M = 7.7.

2. Causes of the excess energy can be different and require separate consideration. We can only say that there is an asymmetrical

distribution of the ratio of the horizontal and vertical components of the stress tensor when a layer at a depth of horizontal stresses is growing at a faster rate than vertical. This leads to the creation of efforts upwards at an angle of 45° – 55° depths of the continental plate, and not by the PP, as it has traditionally been considered.

3. This force effect leads to the formation of zones of increased stress or denser rocks (set according to seismic tomography). When exceeding some threshold voltages failure occurs at the boundary of the medium plates in the form of reverse faults and displacement of large blocks in the upper crust in the direction of least resistance. According reconstruction earthquake focal that the main axis of the compressive stress change their orientation [7] is approximately 90° in the oceanic region for the gutter plate.

4. On the eastern border of the continental plate uplift occurs with dextral shear component. In this part of the plate "leans" on the western part of the ocean, making it subhorizontal tensile stress. Such destruction occurs at intervals of about once every 40 a in the seismic gap. Continental plate like a crocodile "devours" the oceans, causing it to sink down the edge portion. This may explain a series of faults and grabens lying in a gutter part of the oceanic plate.

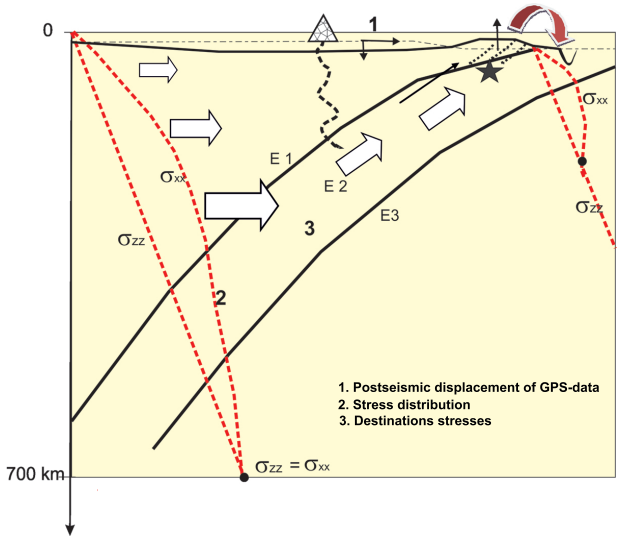

Fig. 1.: Geodynamic model of the development process in the earthquake Tohoku-Oki. 1 - Earth's surface before earthquake, 2 - after the earthquake. The dotted line shows the diagrams of the vertical and horizontal stresses in the continental plate and the oceanic. Elastic module E2 » E1> E3, where the indices 1 - rocks of the continental plate, 2 - zone of elastic rocks seismic tomography data, 3 - upper mantle rocks.

References

1. Shestakov N., Takahashi H., Ohzono M. and other. Analysis of the far-field crustal displacements caused by the 2011 Great Tohoku earthquake inferred from continuous GPS observations. Tectonophysics. 524–525 (2012) 76–86.

2. Mark Simons, Sarah E. Minson, A. Sladen and other. The 2011 Magnitude 9.0 Tohoku-Oki Earthquake: Mosaicking the Megathrust from Seconds to Centuries. Science. Vol.332. 2011.

3. Tong P., Zhao D. and Yang D. Tomography of the 2011 Iwaki earthquake (M 7.0) and Fukushima nuclear power plant area. Solid Earth, 3, 43–51, 2012.

4. http://earthquake.usgs.gov/earthquakes/eqarchives/year/m

5. The Geospatial Information Authority of Japan (GSI). http://www.gsi.go.jp.

6. Paul Segall. GPS applications for geodynamics and earthquake studies. Annu. Rev. Earth Planet. Sci. 1997. 25:301–36.

7. Rebetsky Y.L., Polec A.Y. Stress state of the lithosphere before the catastrophic earthquake in Japan Tohoku. 11.03.2011. Tectonic seminar. Report of December 17, 2013.http://omts.ifz.ru/17_12_2013.html.

Seismo-thermo-mechanical modeling of subduction zone seismicity

Ylona van Dinther[1], Taras Gerya[1], Luis A. Dalguer[2], P. Martin Mai[3]

[1]*Institute of Geophysics, ETH Zurich, Switzerland*
[2]*Swiss Seismological Service, ETH Zurich, Switzerland, now at SwissNuclear,* [3]*Division of Physical Sciences and Engineering, KAUST, Saudi Arabia*
e-mail: *ylona.vandinther@erdw.ethz.ch*
session: *(Seismo-) Tectonics*

Introduction

Recent megathrust earthquakes, e. g., the 2011 M 9.0 Tohoku and the 2004 M 9.2 Sumatra events, illustrated both their disastrous human and economic impact and our limited physical understanding of their spatial occurrence. To be able to better assess earthquake hazard, it is necessary to improve our physical understanding of what drives these events and what makes them more or less catastrophic. One increasingly important tool to improve our understanding is numerical modeling. However, there was no numerical subduction model that a) includes the three key ingredients of seismic cycle modeling in subduction zones -rate dependent friction, slow tectonic loading, and visco-elastic stress relaxation of medium and mantle- (Wang, 2007), b) allows for the spontaneous propagation of ruptures along naturally emerging paths, also outside the megathrust interface, nor c) links long-term subduction dynamics and relating deformation to the short-term seismogenesis. To improve long-term seismic hazard assessment by overcoming the restricted direct observations in time and space, we developed such a seismo-thermo-mechanical (STM) model. The validation and application of such a physically consistent seismo-thermo-mechanical approach is the objective of this study.

Methodology

This 2D continuum-mechanics based model uses an Eulerian-Lagrangian finite difference framework with similar on- and off-fault physics. We implicitly solve the conservation of mass, momentum, and energy for an incompressible medium with a visco-elasto-plastic rheology. Brittle failure is mimicked through Drucker-Prager plasticity. Rapid slip transients are generated through a local, invariant implementation of strongly rate-dependent friction. The validation of this approach is accomplished through a comparison with a laboratory seismic cycle model (Corbi et al., 2013; van Dinther et al., 2013a).

Results for a more realistic setup resembling Southern Chile

A more realistic geometry and physical setup of the Southern Chilean margin showed that results also agree with a range of seismological, geodetic, and geological observations, albeit at lower coseismic speeds (van Dinther et al., 2013b). The strength of a physically consistent approach is highlighted by the qualitative and, after coseismic slip correction, also quantitative agreement of interseismic and coseismic surface displacements with static GPS displacements (Figure 1). These GPS data were recorded before and during the 2010 M8.8 Maule earthquake and a spatial agreement was obtained without a single data

fitting iteration. These results, moreover, highlight the presence of a second-order flexural bulge within the overriding plate, at distances more than 200 km from the trench. A more detailed study of this phenomenon also revealed a similar bulge following the 1960 Valdivia, 1964 Alaska, and 2011 Tohoku earthquakes. The physical mechanisms governing such a bulge remain obscured, but ongoing study aims to identify these.

This study suggests several interesting implications. Slip deficit is observed to vary from one cycle to the next. On the long-term about 5 % of cyclic deformation is permanently stored within the wedge.

We also observe a self-consistent downdip transition zone arising between 350 °C and 450 °C due to the temperature-dependence of viscosity (and a quartzite flow law). Consequent interseismic locking in relation to a fore-arc Moho limits hypocenter locations to temperatures below 350 °C. Stress relaxation due to ductile shearing limits ruptures from propagating beyond 450 °C. These thermal limits correspond to estimates from thermal modeling and laboratory experiments.

Finally, our modeling results suggest that megathrust should be weak to sustain subduction along the megathrust. To generate events with a recurrence intervals and displacements typical for megathrust earthquakes, pore fluid pressures are suggested to be in the range of 75 % to 99 % of that of solid pressures.

Off-megathrust events

Finally, we exploit the main advantage of this innovative approach; the spontaneous unstable rupturing of off-megathrust events (van Dinther et al., 2014). Shallow off-megathrust subduction events are important in terms of hazard assessment and coseismic energy budget. Their role and spatiotemporal occurrence, however, remain poorly understood.

The characteristics of simulated normal events within the outerrise and splay and normal antithetic events within the wedge (Figure 2a-d) resemble seismic and seismological observations in terms of location, geometry, and timing. Their occurrence agrees reasonably well with both long-term analytical predictions based on dynamic Coulomb wedge theory and short-term quasi-static stress changes resulting from the typically triggering megathrust event. The impact of off-megathrust faulting on the megathrust cycle is distinct, as more both shallower and slower megathrust events arise due to occasional off-megathrust triggering and increased updip locking. This also enhances tsunami hazards, which are amplified due to the steeply dipping fault planes of especially outerrise events (Figure 2e – g).

Conclusions

Despite 3D and temporal limitations, these seismo-thermo-mechanical model results captured a wide range of natural observations and dynamic features. This demonstrates the potential of these physically-consistent models and opens a world of interdisciplinary research between geodynamics and seismology. This can relate to the generation and characteristics of megathrust earthquakes and beyond.

References

Corbi, F., Funiciello, F., Moroni, M., van Dinther, Y., Mai, P.M., Dalguer, L.A., and Faccenna, C. (2013). The seismic cycle at subduction thrusts: 1. insights from laboratory models, JGR, 118(4), 1483-1501, doi:10.1029/2012JB009481.

van Dinther, Y., Gerya, T., Dalguer, L., Corbi, F., Funiciello, F., and Mai, P. (2013). The seismic cycle at subduction thrusts: 2. Dynamic implications of geodynamic simulations validated with laboratory models, JGR. Solid Earth, 118(4), 1502–1525, doi:10.1029/2012JB009479.

van Dinther, Y., Gerya, T.V., Dalguer, L.A., Mai, P.M., Morra, G., and Giardini, D. (2013). The seismic cycle at subduction thrusts: insights

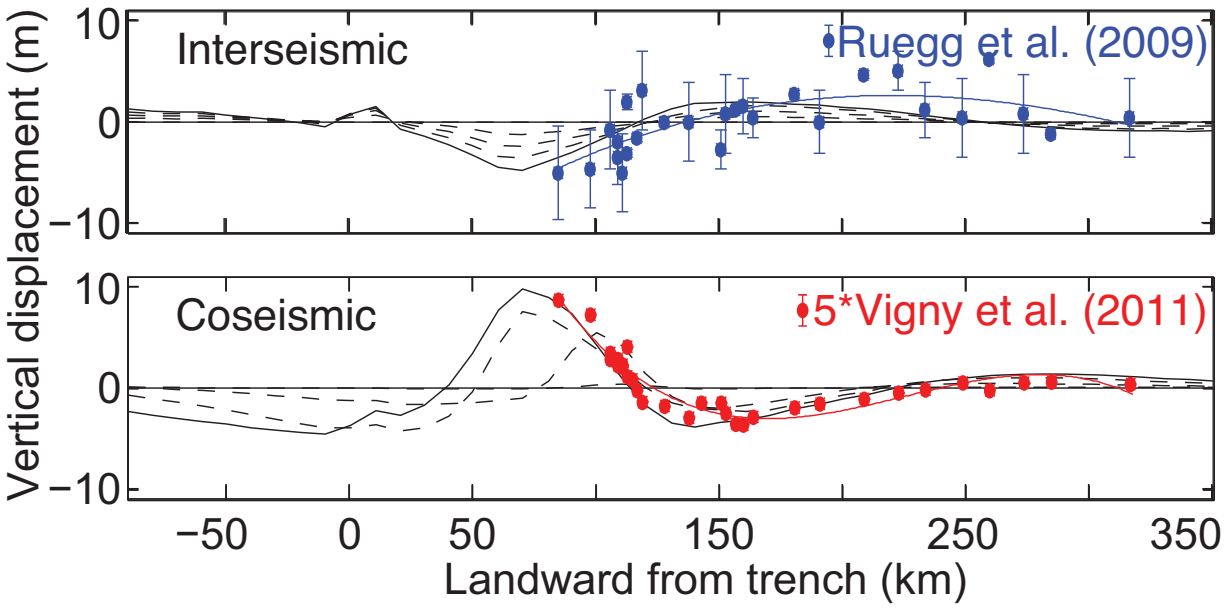

Fig. 1.: Vertical displacements agree spatially with interseismic and coseismic GPS data.

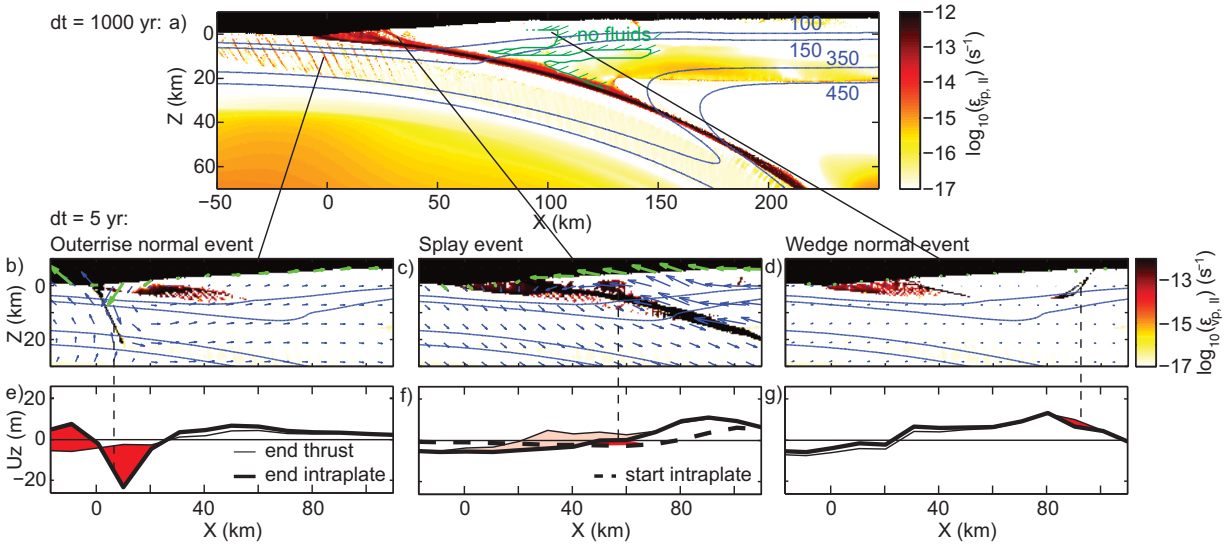

Fig. 2.: a) Long-term off-megathrust variability, b-d) spatiotemporal zooms of each off-megathrust event type, and e-g) accumulated vertical surface displacements w.r.t. the triggering megathrust event.

from seismo-thermo-mechanical models, JGR, 118, 6183-6202, doi:10.1002/2013JB010380.

van Dinther, Y., Mai, P.M., Dalguer, L.A., and Gerya, T.V. (2014). Modeling the seismic cycle in subduction zones: the role and spatiotemporal occurrence of off-megathrust events, GRL, 41 (4), 1194-1201, doi:10.1002/2013GL058886.

Ruegg, J. C., A. Rudlo, C. Vigny, R. Madariaga, J. B. De Chabalier, J. Campos, E. Kausel, S. Barrientos, and D. Dimitrov (2009), Interseismic strain accumulation measured by GPS in the seismic gap between Constitucion and Concepcion in Chile, PEPI, 175.

Vigny, C., et al. (2011), The 2010 Mw 8.8 Maule Megathrust Earthquake of Central Chile, Monitored by GPS, Science, 332 (6036), 1417-1421.

Wang, K. (2007), Elastic and Viscoelastic Models of Crustal Deformation in Subduction Earthquake Cycles, in The Seismogenic Zone of Subduction Thrust Faults, edited by T. Dixon and J. Moore, pp. 540-575, Columbia University Press, New York.

Thermal Expressions of Stick-slip and Creeping Subduction Megathrusts

Kelin Wang[1], Xiang Gao[2]

[1]*Pacific Geoscience Centre, Geological Survey of Canada, Natural Resources Canada, 9860 West Saanich Road, Sidney, British Columbia, V8L 4B2, Canada*
[2]*Key Laboratory of Marine Geology & Environment, Institute of Oceanology, Chinese Academy of Sciences, No. 7 Nanhai Road, Qingdao 266071, China*
e-mail: *kwang@nrcan.gc.ca*
session: *(Seismo-) Tectonics*

The strength of subduction faults and its variations in seismic slip are important to long-term geological deformation as well as earthquake cycles deformation. It is widely assumed that highly seismogenic megathrusts, that is, those that primarily exhibit stick-slip behavior and produce great earthquakes, are stronger than those that creep. Interseismically locked faults are thus described as being "strongly coupled". However, the opposite is also proposed on the basis of the recognition that very rugged subducting seafloor promotes megathrust creep (Wang and Bilek, 2012, 2014). In these rough faults, resistance to creep due to geometrical irregularities is expected to be larger than the failure stress of stick-slip faults. We investigate this paradox by modeling thermal energy dissipated from subduction faults using two-dimensional finite element models constrained by surface heat flow observations.

We first consider two end-member cases (Fig. 1). Japan Trench is a highly seismogenic subduction zone. The subducting seafloor is rather smooth in the area of the 2011 M 9 Tohoku earthquake. Northern Hikurangi is in sharp contrast with Japan Trench. Most of the megathrust is creeping at the subduction rate (100 % creeping ratio), and the subducting seafloor is extremely rugged, featuring a number of subducting seamounts. At both subduction zones, heat flow data provide adequate model constraints.

The model results show that the thermally defined frictional strength of the subduction faults is extremely low, with $\mu' \approx 0.025$ for Japan and 0.13 for Hikurangi (Fig. 1). In comparison, the effective friction of rocks based on the Byerlee's law and at hydrostatic pore fluid pressure is about 0.4. More important is the significant difference between the two subduction zones. The difference is much larger than can be explained by uncertainties, because the highest μ'-value (0.06) marginally acceptable in Japan is still lower than the lowest value marginally acceptable in Hikurangi (0.08) (Fig. 1).

One reason for a lower μ' in Japan is that it primarily represents coseismic fault strength (Fig. 2). As is widely observed in laboratory experiments (Di Toro et al., 2011), faults weaken typically by a factor of three to five when their slip accelerates to seismic rates of $1\,\mathrm{m\,s^{-1}}$, regardless of their frictional behavior at lower rates. In real faults such dynamic weakening may cause complete stress drop in limited areas, but it cannot massively happen, as evidenced by the very small average stress drops in great earthquakes. The Tohoku earthquake exhibits a greater average stress drop than other great earthquakes, but the value is still only about 4 MPa to 7 MPa, although the peak value in a small part of the rupture area might be as high as 40 MPa (Kumagai et al., 2012). At 20 km depth, roughly in the middle of the depth range of the Tokoku rupture,

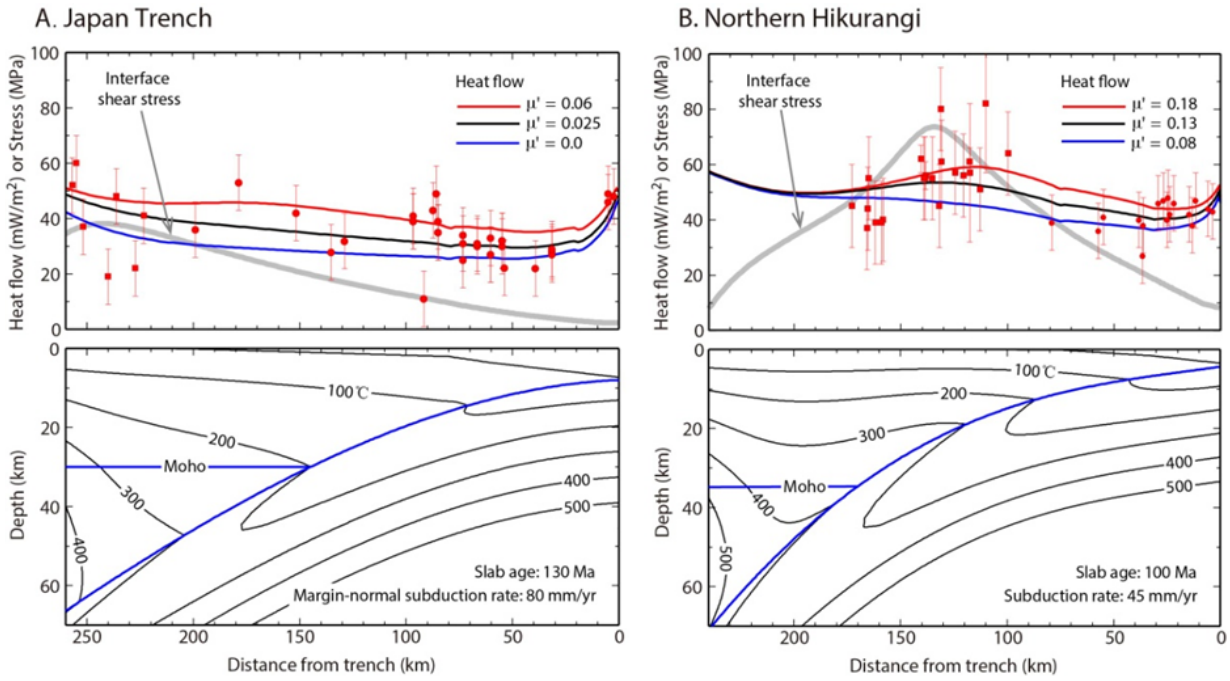

Fig. 1.: Heat dissipation models for Japan Trench and northern Hikurangi. For each subduction zone, top panel shows observed (symbols) and model-predicted (thin lines) surface heat flows and model interface shear stress (thick gray line). Circles and squares indicate marine and land heat flow measurements, respectively (supplementary online text). Bottom panel shows model subsurface temperatures (black contours) and plate interface geometry (blue line).

σ_n (approximated by the weight of the overlying rock column) is about 500 MPa, so that a 5 MPa static stress drop only requires a 0.01 decrease in μ'. In other words, a factor of 1/3 decrease in μ', e. g., from 0.035 to 0.025, is adequate to explain the Japan Trench results. The seemingly small decrease in fault stress is sufficient to reverse the stress state of the upper plate in the rupture area from margin-normal compression to tension (Wang and Suyehiro, 1999), a change that indeed happened as a result of the Tohoku earthquake (Hasegawa et al., 2012).

Therefore, despite the remarkable weakness of subduction faults, the average stress drop in great earthquakes is just a fraction of the average fault strength, albeit a significant fraction. Dramatic dynamic weakening in parts of the fault must be accompanied by much less weakening or even strengthening (negative stress drop) in other parts, such that the average stress drop of the entire rupture zone is much less. An important implication is that the amount of frictional heat is several times the combination of the energy radiated as seismic waves and consumed in permanently deforming rocks around the rupture (Fig. 2). Since the difference in μ' between the two subduction zones cannot be fully explained by dynamic weakening, it must reflect a difference in static fault strength. From observations and theoretical reasoning (Wang and Bilek, 2014), extreme ruggedness of the subducting seafloor such as at northern Hikurangi gives rise to heterogeneous stress and structural environments that promote creep and small earthquakes. But unlike creeping along a smooth fault facilitated by weak gouge, as reported for the creeping segment of the San Andreas fault and shown in Fig. 2 as "weak creep", rough faults creep by breaking and wearing geometrical irregularities in a broad zone of complex internal structure. The integrated resistance to creep is expected to be relatively high, shown in Fig. 2 as "strong creep". Our results in-

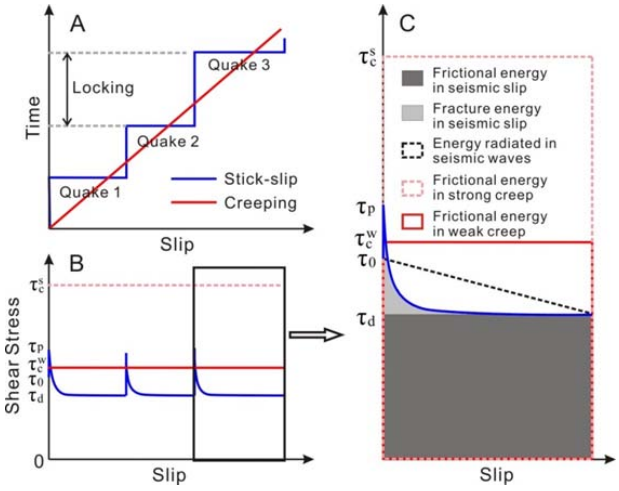

Fig. 2.: Schematic illustration of fault stress and frictional heating for stick-slip and creeping faults. (A) Fault slip history. (B) Fault stress. For stick-slip fault, τ_0 is pre-earthquake stress, τ_p is peak stress, and τ_d is stress during seismic slip (Abercombi and Rice, 2005; Kanamori et al., 2006). τ_c^w and τ_c^s are yield stresses of smooth/weak and rough/strong creeping faults, respectively. (C) A blown-up portion of (B) showing partitioning of energy in seismic slip for stick-slip faults, in comparison with energy dissipated by strong and weak creeping faults.

dicate that the creeping megathrust at northern Hikurangi is indeed stronger than the stick-slip, but much smoother, megathrust at Japan Trench.

We have pursued a global study. Only nine subduction zones including the above two presently have adequate heat flow observations to constrain frictional heating. The results are summarized in Fig. 3 in terms of fault strength results as a function of Mmax, the largest and clearly documented interplate earthquake at each margin. We have added Costa Rica to list. Here we exclude possible tsunami earthquakes, because they occur at a very shallow depth and do not represent the general slip mode of the megathrust. The M_{max} values are meant to provide a crude proxy of seismic slip over the long term. For subduction zones with M_{max} 8.2 to 9.5 (Nankai through Chile in Fig. 3), there is little doubt that fault motion is primarily by stick-slip. For three of the other four subduction zones, although M_{max} may not be an ideal representation of long-term slip behavior, the present locking/creeping state of the megathrust is constrained by modern geodetic measurements. They show significant creep, with northern Hikurangi having the most active creep (~100 % of subduction rate).

Our results suggest a tendency of decreasing μ' with increasing M_{max} or, approximately, less creep. All the highly seismogenic subduction zones in this suite feature rather smooth subducting seafloor, because the igneous crust is devoid of large seamounts or fracture zones, such as Japan Trench and Kamchatka, and/or because large amounts of sediments have evened the bathymetric relief, such as Cascadia and South-Central Chile. The three subduction zones geodetically seen to undergo significant creep all have rugged subducting seafloor. Evidently, it is the weaker but smoother megathrusts that are able to generate great earthquakes. The general correlation between subducting seafloor ruggedness, creeping, and greater heat dissipation, if further verified by future observations, offers a new perspective in assessing earthquake and tsunami hazards for risk mitigation.

References

Abercombie, R. E., J. R. Rice, Geophys. J. Int. 162, 406–424 (2005).

Di Toro, G., et al., Nature 471, 494–498 (2011).

Hasegawa, A., et al., Earth Planet. Sci. Lett. 355-356, 231–243 (2012).

Kanamori, H., L. Rivera, in The missing sinks: Slip localization in faults, damage zones, and the seismic energy budget, Geophys. Monogr. 170, Abercrombie, R., Ed. (America Geophysical Union, Washington DC, 2006), pp. 3–13.

Kumagai, H., N. Pulido, E. Fukuyama, S. Aoi, S., Earth Planets Space 64, 64 –654 (2012).

Wang, K., S. L. Bilek, Tectonophys. 610, 1–24 (2014).

Wang, K., S. L. Bilek, Geology 39, 819–822 (2011).

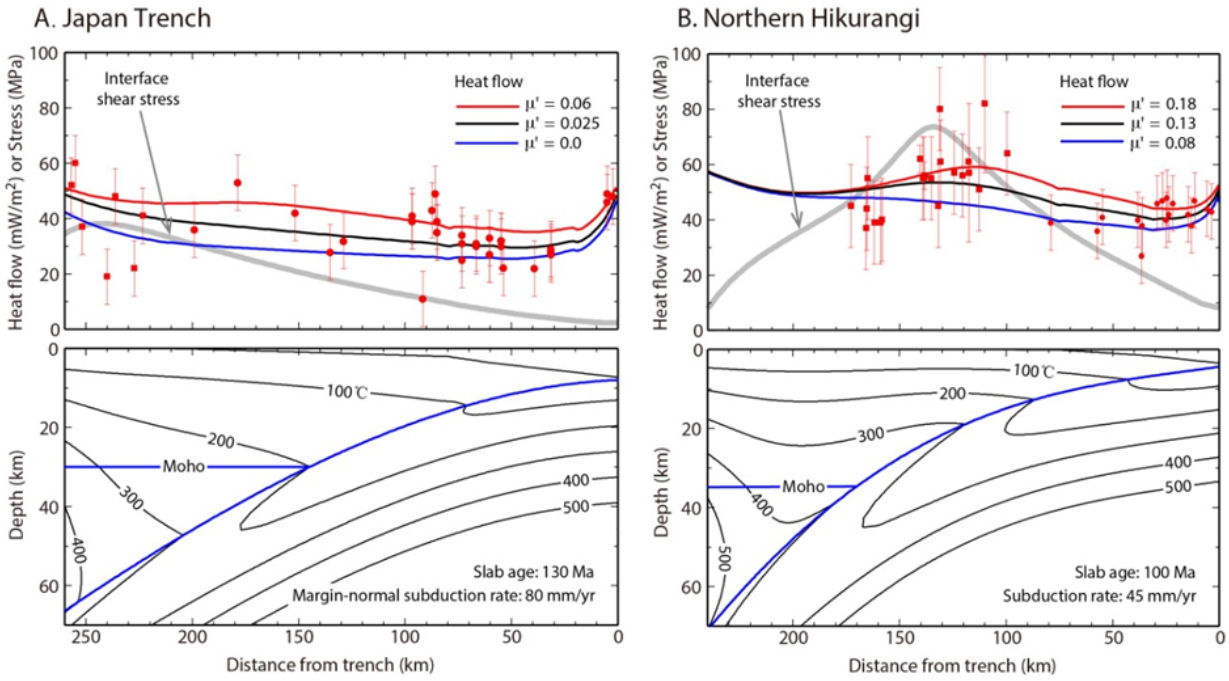

Fig. 3.: Apparent friction of megathrust vs. maximum size of clearly documented interplate earthquakes: 1 – northern Hikurangi, 2 – northern Manila, 3 – Costa Rica, 4 – Kermadec, 5 – Nankai, 6 – Kamchatka, 7 – northern Cascadia, 8 –Japan Trench, 9 – Sumatra, and 10 – south-central Chile (table S 2). The Costa Rica value is an average of previously published results.

Wang, K., K. Suyehiro, Geophys. Res. Lett. 26, 2307–2310 (1999).

Scientific Programme

GeoMod2014 - Conference Outline

Time	31. August	1. September	2. September	3. September
08:45 - 09:00	-	Welcome	-	-
09:00 - 11:00	-	(Seismo-)tectonics (orals)	Volcanism and Volcanotectonics (orals)	Rheology (orals)
11:00 - 13:00	-	(Seismo-)tectonics (posters)	Volcanism and Volcanotectonics (poster)	Rheology (poster)
13:00 - 14:00	-	Lunch break	Lunch break	Lunch break
14:00 - 16:00	-	Tectonics and Surface processes (orals)	Geodynamics (orals)	Fluids and Deformations (orals)
16:00 - 18:00	-	Tectonics and Surface processes (poster)	Geodynamics (posters)	Fluids and Deformations (poster)
18:00 - 21:00	Ice Breaker Party	-	-	-
19:00 - 22:00	-		Joint Conference Dinner	-

GeoMod2014 - Short course on "Constitutive Laws: from Observation to Implementation in Models" by Onno Oncken, Mathias Rosenau, Fabio Corbi, Georg Dresen Erik Rybacki, Stephan Sobolev, and Sascha Brune
Thursday 4 September: 09:00 - 18:00
Friday 5 September: 09:00 - 14:00

GeoMod2014 - Hands-on tutorial on "ASPECT: a next-generation geodynamic modelling software" by Anne Glerum and Juliane Dannberg
Thursday 4 September: 09:00 - 18:00: Tutorial
Friday 5 September: 09:00 - 18:00: ASPECT Strategy Workshop (for Advanced Users) - voluntary

GeoMod2014 Conference Programme (31 August - 3 September)

Sunday 31 August 2014

18:00 - 21:00: Ice Breaker Party at the 'Theaterschiff Potsdam' (Schiffbauergasse 9b, 14467 Potsdam)

Monday 1 September 2014

08:45 - 09:00: Welcome by Prof. Dr. Dr. h.c. Reinhard Hüttl and Prof. Dr. Onno Oncken

09:00 - 11:00: (Seismo-)tectonics Orals (chairs: B. Kaus, O. Oncken)

- 09:00 - 09:30: **Kelin Wang:** *Thermal Expressions of Stick-slip and Creeping Subduction Megathrusts* (keynote)
- 09:30 - 10:00: **Bertrand Maillot:** *The long-term Evolution of Fold-and-Thrust Belts: Consistency of Numerical Approaches and Physical Experiments* (keynote)
- 10:00 - 10:20: **Tasca Santimano** et al.: *Smart or Beautiful? Accretionary wedge evolution seen as a competition between minimum work and critical taper*
- 10:20 - 10:40: **Lorenzo Bonini** et al.: *The role of pre-existing frictional weaknesses on the propagation of extensional faults*
- 10:40 - 11:00: **Ylona van Dinther** et al.: *Seismo-thermo-mechanical modeling of subduction zone seismicity*

11:00 - 13:00: (Seismo-)tectonics Posters (chairs: B. Kaus, O. Oncken)

13:00 - 14:00: Lunch break

14:00 - 16:00: Tectonics and Surface processes Orals (chairs: F. Graveleau, N. Hovius)

- 14:00 - 14:30: **Ritske Huismans:** *Interaction and feedback between surface processes and mountain building* (keynote)
- 14:30 - 15:00: **Stéphane Dominguez:** *Joint analogue modelling of marine and terrestrial geological processes: state of the art and new developments* (keynote)
- 15:00 - 15:15: **Utsav Mannu** et al.: *Dynamic Modelling of Accretionary Prisms and Stratigraphy of Forearc basins*
- 15:15 - 15:30: **Karen Leever:** *3D Analogue Modelling of the Effect of Fan Sedimentation on Accretionary Wedge Dynamics – the Magdalena Fan case, South Caribbean Margin, Colombia*
- 15:30 - 15:45: **Frank Zwaan**, Guido Schreurs: *4D Transfer Zone Modeling in Continental Rift Systems*
- 15:45 - 16:00: **Sergei Medvedev**, Ebbe H. Hartz: *Evolution of topography of post-Devonian Scandinavia: Effects and rates of erosion*

16:00 - 18:00: Tectonics and Surface processes Posters (chairs: F. Graveleau, N. Hovius)

Tuesday 2 September 2014

09:00 - 11:00: Volcanism and Volcanotectonics Orals (chairs: O. Galland, E. Holohan)

- 09:00 - 09:30: **Rikke Pedersen:** *Surface deformation simulations of volcanic and tectonic processes in Iceland* (keynote)
- 09:30 - 10:00: **Olivier Roche**, Yarko Niño: *Mechanisms of entrainment of a granular substrate by pyroclastic density currents: insights from laboratory experiments and models, and implications for flow dynamics* (keynote)
- 10:00 - 10:15: **Rosanne Heistek** et al.: *Temporal changes in mantle wedge geometry and magma generation processes in the Central Andes: towards linking petrological data to thermomechanical models*
- 10:15 - 10:30: **Francesco Maccaferri** et al.: *The gravitational unloading due to rift depression: A mechanism for the formation of off-rift volcanoes in (continental) rift zones*
- 10:30 - 10:45: **Lola Chanceaux**, Thierry Menand: *Solidification effects on sill formation: an experimental approach*
- 10:45 - 11:00: Max Gallagher, **Ben Kennedy** et al.: *Megatsunami generation from caldera subsidence*

11:00 - 13:00: Volcanism and Volcanotectonics Posters (chairs: O. Galland, E. Holohan)

13:00 - 14:00: Lunch break

14:00 - 16:00: Geodynamics Orals (chairs: F. Funiciello, S. Sobolev)

- 14:00 - 14:30: **Anne Davaille:** *Plumes to Plate Tectonics: Insights from Laboratory Experiments* (keynote)
- 14:30 - 15:00: **Bernhard Steinberger** et al.: *On the relation between plate tectonics, large-scale mantle flow and mantle plumes: Some recent results and many open questions* (keynote)
- 15:00 - 15:15: **Paul J. Tackley** et al.: *Influence of Melting on the Long-Term Thermo-Chemical Evolution of Earth's Deep Mantle*
- 15:15 - 15:30: **Maria V. Chertova** et al.: *3-D numerical modeling of subduction evolution of the western Mediterranean region*
- 15:30 - 15:45: Tobias Baumann, **Boris Kaus**, A. Popov: *Constraining the rheology of the lithosphere through geodynamic inverse modelling*
- 15:45 - 16:00: **Elisa Calignano** et al.: *Strain localization during compression of a laterally heterogeneous lithosphere*

16:00 - 18:00: Geodynamics Posters (chairs: F. Funiciello, S. Sobolev), Methods and Materials Posters (chairs: M. Frehner, M. Rosenau)

19:00 - 22:00 Joint conference dinner in Potsdam on the ship 'Belvedere' (Lange Brücke 6, 14467 Potsdam)

Wednesday 3 September 2014

09:00 - 11:00: Rheology Orals (chairs: G. Dresen, H. Sone)

- 09:00 - 09:30: **Yuri Fialko:** *Numerical models of ductile roots of mature strike-slip faults* (keynote)
- 09:30 - 10:00: **Laurent Montési:** *Localization processes on Earth, Mars, and Venus* (keynote)
- 10:00 - 10:20: **Suzon Jammes** et al.: *Localization of deformation in a polymineralic material*
- 10:20 - 10:40: **Sebastian P. Müller** et al.: *Rheology of bubble- and crystal-bearing magma: new analogue experimental data and an effective-medium model*
- 10:40 - 11:00: **Maria A. Nikolinakou** et al.: *Modeling stress evolution around a rising salt diapir*

11:00 - 13:00: Rheology Posters (chairs: G. Dresen, H. Sone)

13:00 - 14:00: Lunch break

14:00 - 16:00: Fluids and Deformations Orals (chairs: S. Miller, M. Moreno)

- 14:00 - 14:30: **Boris Galvan** et al.: *Towards a general simulation tool for complex fluid-rock lithospheric processes: merging pre-processing, processing and post-processing in state-of-the-art computational devices* (keynote)
- 14:30 - 15:00: **Takeshi Tsuji:** *Digital rock physics: Insight into fluid flow and elastic deformation of porous media* (keynote)
- 15:00 - 15:15: **Thomas Heinze** et al.: *Numerical Modelling of earthquake swarms in the Vogtland / West- Bohemia*
- 15:15 - 15:30: **Samuel Angiboust** et al.: *Effect of Fluid Circulation on Intermediate-Depths Subduction Dynamics: From Field Observations to Numerical Modelling*
- 15:30 - 15:45: Magdalena Scheck-Wenderoth, **Judith Sippel** et al.: *Heat transport mechanisms at different scales – a 3D modelling workflow*
- 15:45 - 16:00: **Antoine Jacquey** et al.: *Modelling of fractured reservoirs: Fluid-rock interactions within fault domains*

16:00 - 18:00: Fluids and deformations Posters (chairs: S. Miller, M. Moreno)

The posters will be presented during the entire conference. Each poster session starts with a 1-2 min. short presentation of all participating posters.

GeoMod2014 - Short course on "Constitutive Laws: from Observation to Implementation in Models"

Thursday 4 September 2014

Morning Session: Onno Oncken, Mathias Rosenau, and Fabio Corbi

- 09:00 - 10:00: **Onno Oncken:** Observing deformation kinematics and localization: Observations from the field, geophysical imaging, and geodetic monitoring
- 10:00 - 10:15: Coffee Break
- 10:15 - 11:00: **Mathias Rosenau:** Rheology of rock analogues 1: Elastoplasticity and its application in seismotectonic simulation
- 11:00 - 11:15: Coffee Break
- 11:15 - 12:00: **Fabio Corbi:** Rheology of rock analogues 2: Viscoelasticity and its application in seismotectonic simulation
- 12:00 - 13:00: **Visit to the GFZ Analogue Lab**

13:00 - 14:00: Lunch break

Afternoon Session: Georg Dresen and Erik Rybackii

- 14:00 - 15:15: Rheology of the lower crust : Reconciling laboratory data and field observations
- 15:15 - 15:30: Coffee Break
- 15:30 - 16:45: **Visit to the GFZ rock mechanics lab**
- 16:45 - 17:00: Coffee Break
- 17:00 - 18:00: Rock fracture processes and stick slip sliding –What do we learn from analyzing nanofemto seismicity?

Friday 5 September 2014

Morning Session: Stephan Sobolev and Sascha Brune

- 09:00 - 10:00: **Stephan Sobolev:** Rheology and geodynamic modeling: key controls in plate tectonics and beyond
- 10:00 - 10:15: Coffee Break
- 10:15 - 11:30: **Sascha Brune:** Rock rheology in numerical models: PC exercises and application to rift dynamics
- 11:30 - 11:45 Coffee Break
- 11:45 - 12:30: **Stephan Sobolev:** Rheology and cross-scale modeling: towards understanding of great earthquakes
- 12:30 - 13:00: Discussion

13:00 - 14:00: Lunch and end of the short course

GeoMod2014 – Hands-on tutorial on"ASPECT: a next-generation geodynamic modelling software" by Anne Glerum and Juliane Dannberg

Thursday 4 September 2014

08:30 - 9:00: Registration

- 09:00 - 10:00: **Tutorial 1:** First Steps – Compiling and Running ASPECT, **Lecture:** How to run and visualize simple models
- 10:00 - 11:15: **Lecture** ASPECT – A next-generation geodynamic modelling software, **Tutorial 2:** Convection in a 2D box
- 11:15 - 11:30: Coffee Break
- 11:30 - 13:00: **Tutorial 3:** Using the adaptive mesh refinement and spherical shell geometry **Lecture:** How to run and visualize simple models

13:00 - 14:00: Lunch break

- 14:00 - 15:15: **Tutorial 4:** Using the adaptive mesh refinement and spherical shell geometry and using the function parser
- 15:15 - 15:30: Coffee Break
- 15:30 - 17:00: **Tutorial 5:** Averaging at the example of subduction and using a “sticky air” layer
- 17:00 - 18:00: **Voluntary:** Installing ASPECT on personal computers

18:30: Joint Dinner (to be payed by the participants)

Friday 5 September 2014

09:00 - 18:00: ASPECT Strategy Workshop for Advanced Users: Perspectives for Modelling with ASPECT

Index